ANNUAL REVIEWS

Annual Review of Biomedical Engineering

Simulating Outcomes of Cataract Surgery: Important Advances in Ophthalmology

Susana Marcos,[1] Eduardo Martinez-Enriquez,[1] Maria Vinas,[1] Alberto de Castro,[1] Carlos Dorronsoro,[1,2] Seung Pil Bang,[3] Geunyoung Yoon,[3] and Pablo Artal[4]

[1]Instituto de Óptica "Daza de Valdés," Consejo Superior de Investigaciones Científicas (IO-CSIC), Madrid 28006, Spain; email: susana@io.cfmac.csic.es

[2]2EyesVision, Madrid 28760, Spain

[3]Flaum Eye Institute, The Institute of Optics, Center for Visual Science, Department of Biomedical Engineering, University of Rochester, Rochester, New York 14632, USA

[4]Laboratorio de Óptica, Universidad de Murcia, Murcia 30100, Spain

Annu. Rev. Biomed. Eng. 2021. 23:277–306

First published as a Review in Advance on April 13, 2021

The *Annual Review of Biomedical Engineering* is online at bioeng.annualreviews.org

https://doi.org/10.1146/annurev-bioeng-082420-035827

Keywords

intraocular lens, cataract surgery, anterior segment imaging, optical coherence tomography, visual simulation, adaptive optics

Abstract

As the human eye ages, the crystalline lens stiffens (presbyopia) and opacifies (cataract), requiring its replacement with an artificial lens [intraocular lens (IOL)]. Cataract surgery is the most frequently performed surgical procedure in the world. The increase in IOL designs has not been paralleled in practice by a sophistication in IOL selection methods, which rely on limited anatomical measurements of the eye and the surgeon's interpretation of the patient's needs and expectations. We propose that the future of IOL selection will be guided by 3D quantitative imaging of the crystalline lens to map lens opacities, anticipate IOL position, and develop fully customized eye models for ray-tracing-based IOL selection. Conversely, visual simulators (in which IOL designs are programmed in active elements) allow patients to experience prospective vision before surgery and to make more informed decisions about which IOL to choose. Quantitative imaging and optical and visual simulations of postsurgery outcomes will allow optimal treatments to be selected for a patient undergoing modern cataract surgery.

Contents

Presbyopia: age-related loss of accommodation (capability to focus on objects dynamically) resulting from stiffness of the crystalline lens

Cataract: cloudiness in the crystalline lens of the eye that develops with age

Intraocular lens (IOL): artificial lens implanted into the eye that replaces the cataractous crystalline lens, restoring transparency and refractive errors

1. INTRODUCTION

1.1. Presbyopia and Cataract

When the human eye ages, the crystalline lens loses its flexibility to dynamically focus near and far, and later it becomes cloudy, resulting in significant vision loss (**Figure 1**). The loss of accommodation, known as presbyopia, becomes noticeable at approximately age 45 and occurs in nearly 100% of the population (1). Changes in the geometry and the material properties (such as the refractive index) of the crystalline lens due to age result in changes in its optical properties, in particular a shift of its spherical aberration toward positive values (whereby peripheral rays focus closer than central rays do) (2–5), which can be assessed by aberrometry techniques (6). The opacification of the crystalline lens, known as cataract, generally occurs after age 65 (**Figure 1**), although there are cases of congenital cataract, or it can develop at a young age after eye injury, eye inflammation, or diabetes (7).

Presbyopia compromises vision at a relatively young age, affecting productivity and quality of life and requiring the use of near-vision aids (such as reading glasses or bifocal or progressive addition lenses) (8). Alternative solutions for presbyopia include monovision (correction of an eye for near vision and the contralateral eye for far vision), multifocal contact lenses, multifocal intraocular lenses (IOLs), and expectedly in the future, accommodating IOLs that mimic the focusing capacity of the crystalline lens (9–12).

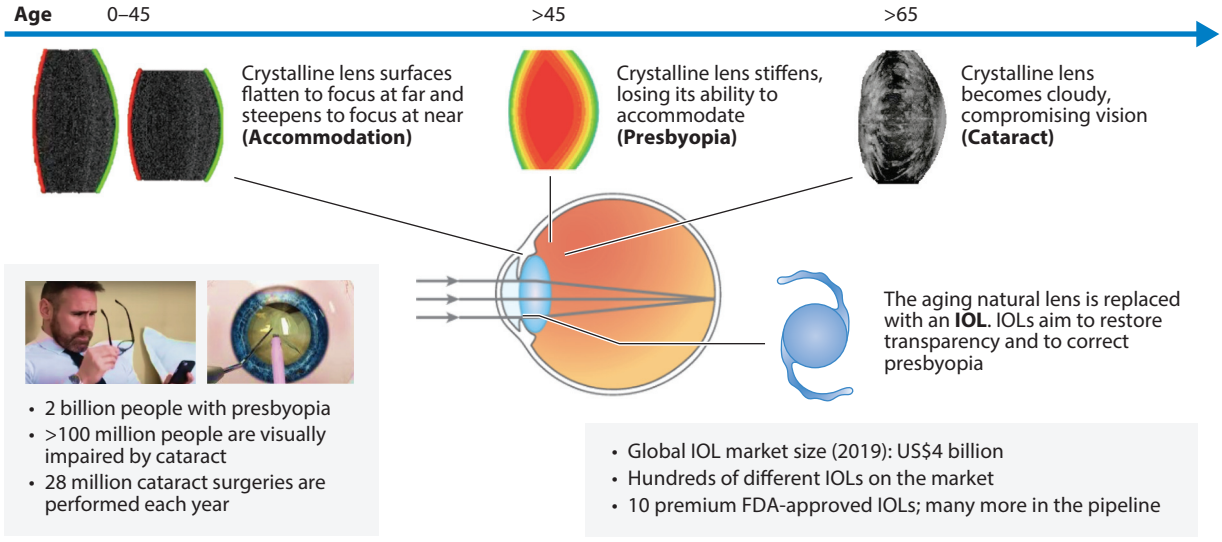

Figure 1

Aging of the crystalline lens and methods of correction. The young crystalline lens of the eye can dynamically reshape to focus at near and at far (accommodation) [*upper-left images* are OCT cross sections of the crystalline lens of the eye viewing at far at infinity (*left*) and at near at 20 cm (*right*); obtained as described in Reference 79]. As the eye ages, the crystalline lens stiffens and its index of refraction becomes more uniform (*upper-middle image*; obtained using methods described in Reference 4). At approximately age 45, the amplitude of accommodation is highly reduced (presbyopia). Later in life, the crystalline lens opacifies (cataract) (*upper-right image*; 3D-OCT image of cataractous crystalline lens, obtained as described in Reference 63). Presbyopia and cataract are highly prevalent conditions that affect millions worldwide. The global size of the IOLs market increases (compound annual growth rate) at 5.54%, with a marked increase in the so-called premium IOLs, which aim to improve optical quality beyond that of standard lenses (e.g., multifocal IOLs to correct presbyopia) (154). Abbreviations: 3D OCT, three-dimensional optical coherence tomography; FDA, US Food and Drug Administration; IOL, intraocular lens.

Cataract continues to be a global burden. It is considered by the World Health Organization to be a priority eye disease, and it is responsible for 51% of blindness in the world and contributes to more than 90% of the total disability-adjusted life years (13). The treatment for cataract is surgery and cataract surgery is very successful at restoring eyesight (14). In addition, new low-cost technologies are helping overcome accessibility barriers in developing countries (15, 16). As life expectancy continues to increase, the number of people with cataracts is expected to grow. To date, with approximately 28 million cataract procedures performed annually worldwide, cataract surgery is the most frequently performed surgical procedure in most hospitals around the world (17). Cataract surgery almost invariably entails extracting the opacified crystalline lens and inserting an artificial lens (see the IOL in **Figure 1**) into the emptied capsular bag. Modern cataract surgery is highly noninvasive, requiring only small incisions (approximately 2 mm or less) to insert auxiliary instrumentation, viscoelastic substances and the folded IOL (generally by using an injector), and a circular window (capsulorhexis) in the anterior lens capsular bag. The opacified lens material is broken down into smaller pieces with the use of an ultrasonic handpiece, a technique called phacoemulsification. In 2019, femtosecond lasers were introduced with a similar purpose and also to create the capsulorhexis (18). Improvements to the surgical technique have undoubtedly resulted in safer and more predictive cataract surgeries. However, other advances have the potential to revolutionize cataract surgery as we know it today. While the primary goal of cataract surgery has traditionally been to restore lens transparency, cataract surgery has also become a refractive surgery procedure, as selection of the proper IOL power corrects refractive errors and

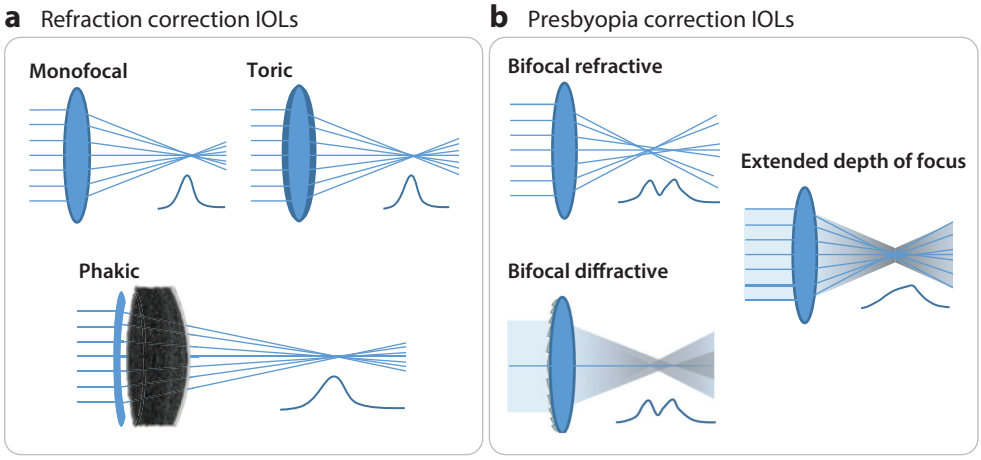

Figure 2

Principles of operation of IOLs. IOLs can be classified according to the principle of operation, or correcting condition. (*a*) Refractive lenses exhibit smooth surfaces and generally include monofocal IOLs (state-of-the-art IOLs that have aspheric surfaces and correct defocus and, in most cases, some corneal spherical aberration), toric IOLs (which correct both defocus and astigmatism), some EDOF lenses (which expand depth of focus), and phakic IOLs (which are implanted in front of the preserved natural crystalline lens generally to correct for high myopia). (*b*) Multifocal lenses provide the eye with far and near (sometimes also intermediate) vision to compensate for presbyopia, superimposing sharp and out-of-focus images on the retina. They can be refractive (generally zonal, with zones devoted to near vision and far vision) or diffractive (i.e., containing diffractive elements that operate by interference and diffraction). Abbreviations: EDOF, extended depth of focus; IOL, intraocular lens.

modern aspheric IOLs correct spherical aberration of the cornea (19). Furthermore, new IOL designs have been developed to produce multiple foci (and to provide functional vision at multiple distances, using refractive or diffractive optics), also with the aim of correcting presbyopia (20, 21) (**Figure 2**). Replacement of the crystalline lens with an IOL is increasingly being performed before a cataract develops, in so-called clear lens extraction or refractive lens exchange procedures (22).

The sophistication of lens designs has not always been accompanied by sophisticated biometry methods and IOL selection strategies, with inaccuracies and imprecision in preoperative measurements resulting in residual defocus (23). Traditionally, diagnostic technologies prior to cataract surgery involve slit-lamp imaging (to characterize the level of opacity in the crystalline lens), eye axial length measurements [using either ultrasound techniques or, more recently, a noncontact optical technique called low-coherence interferometry (24, 25)], and corneal curvature measurements (using keratometry techniques) (**Figure 3**). These measurements are typically introduced in simple formulas to calculate the IOL power to be implanted. There is ample room for improvement in the way cataracts are diagnosed and IOLs are selected. Current anterior segment imaging techniques do not offer 3D maps of lens opacities or quantitative 3D geometric parameters of the crystalline lens. Current methods of IOL selection rely on important assumptions regarding corneal shape or estimated lens position, which may lead to significant refractive errors and degraded retinal image. For example, deviations of >1.75 diopter (D) have been reported when the standard IOL-power-calculating formulas are applied in post-LASIK patients (26). Also, Norrby (23) reported that inaccuracies in the estimation of lens position (the largest contributor to error) along with axial length may result in a residual error of 0.6 D.

In this article, we review new optical technologies that map the full geometry and structure of the eye prior to surgery, presenting a 3D view of the crystalline lens and custom eye models.

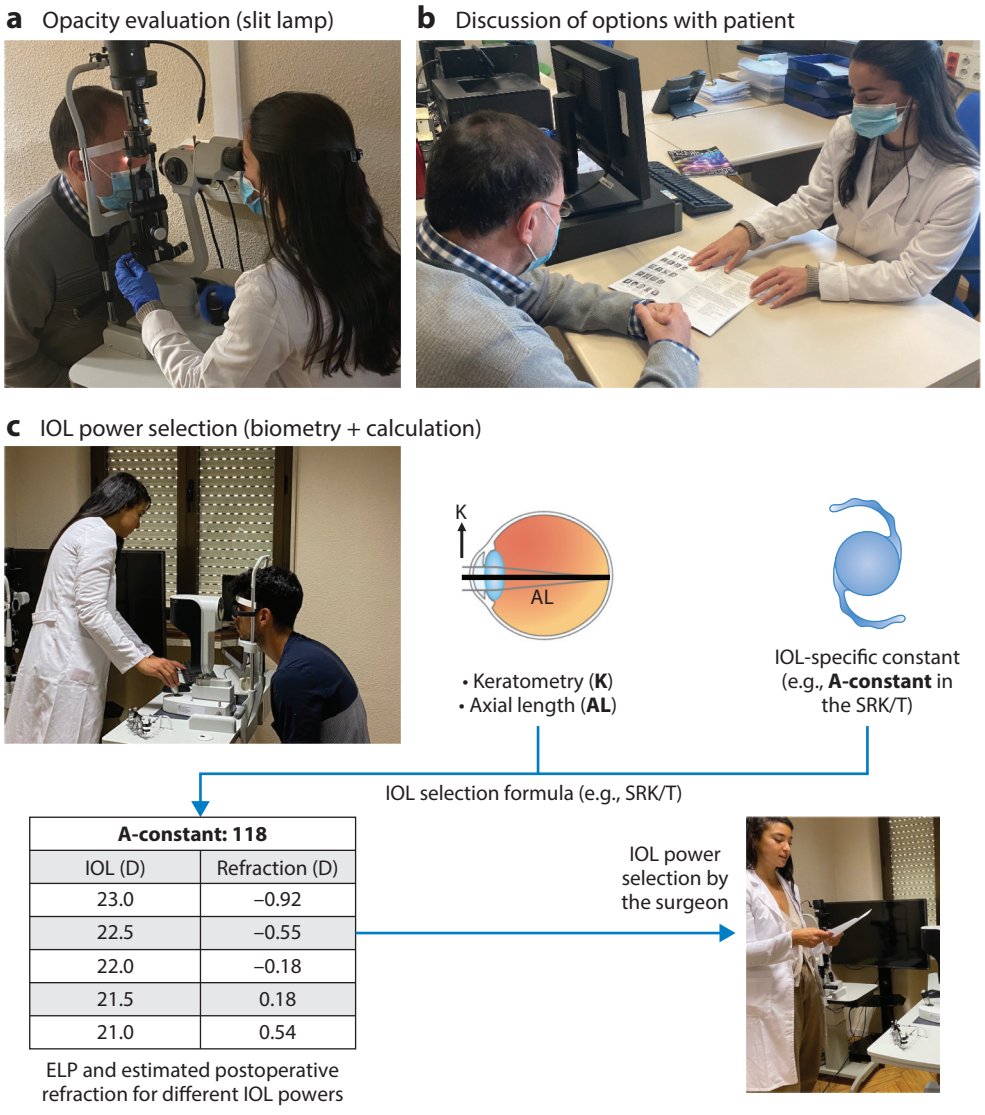

Figure 3

Standard steps prior to IOL implantation. (*a*) A slit-lamp examination is performed to assess the presence of opacities. (*b*) The doctor explains to a patient the need for cataract surgery and potential surgical alternatives to correct for refractive errors and presbyopia, and discusses different available IOL designs (i.e., monofocal, multifocal) that may suit the patient's needs. The IOL type is then identified and selected. (*c*) Standard clinical procedures for calculating IOL power involve preoperative measurement of corneal curvature (using keratometry) and axial length (generally using low-coherence interferometry). The top-left image depicts a patient being measured with a commercial biometer Lenstar LS 900 (Haag-Streit). A constant parameter associated with the lens (i.e., A-constant for the SRK/T formula) is introduced, and residual spherical equivalent errors are calculated for different lens powers. The clinician may decide to slightly undercorrect or fully correct the patient after visual needs are discussed (*bottom-right image*). Abbreviations: D, diopter; ELP, effective lens position; IOL, intraocular lens.

Retinal image quality: quality of the image projected onto the retina by the cornea and lens; defined by performance metrics

These models allow comprehensive surgical planning and simulations of the optical performance of specific solutions in-eye, customized to the patient's eye anatomy. Furthermore, IOLs are permanent treatments; however, patients do not have the opportunity to experience prospective postoperative vision with different IOL designs (e.g., standard or premium IOLs aimed at correcting presbyopia; **Figure 2**). In settings where options are possible (e.g., public health care systems with compatible reimbursement models or private settings), the decision of which IOL to implant is based on discussions about a patient's needs and expectations, but it is hard for the patient to imagine how they are going to see with the IOLs that are selected.

Realistic simulations of the outcomes of cataract surgery, which would allow the patient to experience and judge the quality of their vision prior to IOL implantation, will undoubtedly increase surgeon and patient confidence. Surgeons and patients can select the IOL that provides the best perceived vision, avoiding IOL designs with which the patient will not be happy. In a 2012 report (27) analyzing refractive data of more than 17,000 eyes after cataract surgery, emmetropia was achieved in only 55% of the eyes for which it was targeted. Furthermore, in a study of 257 pseudophakic patients that underwent IOL explantation due to a high level of dissatisfaction, incorrect lens power and intolerance for multifocal vision quality accounted for 12.8% and 6.2% of the cases for explantation and lens exchange, respectively (28). Studies have reported rates of multifocal IOL exchange among dissatisfied patients ranging from 0.85% to 7% (29). Besides, premium IOLs have a market penetration rate of only 17.8% [according to an analysis of 85 US metropolitan areas in 2020 (30)] owing to lack of confidence of surgeons and patients. We envision that the use of quantitative eye imaging technologies, simulations, and new strategies for eye selection will result in more accurate correction and increased satisfaction.

1.2. Intraocular Lenses

In the last few years, there has been a spectacular increase in the number of IOL designs available for presbyopia and cataract surgeries (21, 31, 32). Three major factors determine the performance of an IOL: material, IOL platform, and IOL surface geometry. Material is critical to biocompatibility, transparency, biomechanics, and optical properties. IOL platform includes haptics and edge design, which are critical to stability and for avoiding posterior capsular opacification. IOL surface geometry determines the optical quality of the lens (33). Important advances in material developments (in both hydrophobic and hydrophilic materials) have reduced proliferation and migration of fibroblasts that produce posterior capsular opacification and have avoided calcification or microvacuoles (glistenings) in the IOL (34). Furthermore, IOLs that could ultimately restore dynamic accommodation (the accommodating IOLs) rely heavily on compliant materials and efficient mechanical design (35–37). However, in all cases, the IOL geometric design directly affects the optical quality of the IOL and, in combination with the patient's cornea, the retinal image quality and therefore the visual quality of the patient after implantation. Designing and simulating performance with an IOL entail defining the geometry of the lens surface. Around a decade ago, IOL surfaces were designed to be spherical, defined by anterior and posterior radii of curvature, with those values along with the refractive index of the material determining the optical power of the IOL. Spherical monofocal IOL designs induce positive spherical aberration, which adds to the generally positive spherical aberration of the patient's cornea (38). Aspheric-surface monofocal IOLs are designed to induce negative spherical aberration and to compensate (at least in part) for the positive spherical aberration of the cornea, therefore optimizing retinal image quality at best focus (19). Optical design and simulation methods allow the surgeon to predict the performance of these IOLs, which are designed to induce a certain amount of spherical aberration (aspheric IOLs), to correct astigmatism (toric IOLs) (**Figure 2**), or to achieve a determined target image quality (i.e., optimized across the visual field or in a range of focus).

Besides monofocal and extended depth-of-focus (EDOF) IOL designs, multifocal IOLs produce foci at near (sometimes also at intermediate) and at far (21, 39), thus producing visual functionality at different distances in the presbyopic patient (**Figure 2**). Multifocal IOLs (which can be refractive or, more often, diffractive) operate under the principle of simultaneous vision, whereby focused and out-of-focus images of the same object superimpose, reducing (to some extent) not only the optical quality at far but also the need for near-vision aids. In all lenses, computer eye models (centered and with generic corneas) are used, at least in ideal conditions, to evaluate the IOL design, simulating the through-focus performance of the lens (40). IOLs are also bench tested (using American National Standards Institute–standard physical model eyes) to verify compliance of the manufacturing process (41–44). Although generic bench testing and computer eye model simulations help us understand the intended IOL optical performance, they are unable to capture the subtleties of the interactions between a real patient's cornea and the IOL. In addition, optical techniques alone do not measure the influence of perceptual aspects on a patient's tolerance for a certain degradation in image quality, missing an important component in the final selection of a given IOL.

1.3. State of the Art in Intraocular Lens Power Calculations

An important requirement in standard cataract surgery is that an appropriate IOL power be selected so that focused images of an object fall on the retina at far distance. Simulation and IOL selection planning tools based on 3D quantitative measurements of the eye's anatomy have still not reached the level of general practice. Instead, IOLs are selected on the basis of paraxial equations and regression models, with generally limited quantitative input from the eye's biometry/geometry.

The first estimations of the IOL power used paraxial optics (45), a first-order approximation in which the optical surfaces change only the vergence of the beams of light. With this approximation, the optical power of the IOL can be calculated from eye parameters such as the corneal power, the axial length, and the effective lens position (ELP) (i.e., the distance from the cornea to the IOL). Corneal power is traditionally obtained from keratometry techniques (based on the estimation of the magnification of images reflected on the cornea), but assumptions need to be made regarding the contributions of the posterior corneal surface and the index of refraction to corneal power (introduced in the form of the corneal keratometric index). The accuracy of axial measurements (particularly the axial length of the eye) has improved, especially when shifting from contact ultrasound techniques to noncontact optical techniques (low-coherence interferometry) (24, 25). According to Norrby (23), errors in the estimation of the ELP account for the largest source of error in postoperative refraction (35%), and it appears well established that improvement in the refractive outcome requires better methods for predicting postoperative position. A scaling factor for ELP dependent on the axial length was introduced in a second generation of theoretical formulas. The most frequently used formulas today (third-generation formulas) are based on measurements of the eye's axial length and corneal curvature and require constants (provided by the manufacturer and frequently adjusted by the surgeon) that are specific to each lens model and formula: surgeon factor in the Holladay formula (46), A-constant in the SRK/T formula (47), and personalized anterior chamber depth (ACD) in the Hoffer Q formula (48). Predictions of the IOL position are usually based on initial and generally large data sets, but the prediction models [except, for example, the Haigis formula (49)] do not incorporate preoperative ACD measurements. The Olsen formula is based on two additional measurements—preoperative refraction and lens thickness (LT) (50, 51). Other formulas, such as the Holladay II formula, include the patient's age and the horizontal white-to-white corneal diameter (52), and the

Barrett formula uses a theoretical model eye whereby ACD is related to axial length and corneal curvature and is also determined by the relationship between the A-constant and a lens factor, with the ELP introduced as a variable (53). According to clinical studies, the SRK/T formula is recommended for very long eyes, whereas the Hoffer Q formula is recommended for very short eyes. The so-called fourth-generation formulas (Barrett, Holladay II, and Haigis), which include more variables, should provide the highest accuracy over the full range of axial lengths (54).

Most of the general equations fail in patients whose eye geometry falls outside normal population values (e.g., patients who had undergone corneal refractive surgery or patients with very long or very short eyes), and they rely heavily on updates of adjusting factors (such as the A-constant) or specifically designed formulas (i.e., the double-K method) (55). Instead, computer eye models that simulate the true retinal image quality on the basis of patient-specific geometric information will more accurately calculate the optimal IOL power and a more customized selection of an IOL. These simulations will benefit the selection of both standard monofocal IOLs and premium IOLs (i.e., toric IOLs for correcting astigmatism, EDOF IOLs, or multifocal IOLs) (**Figure 2**). **Figure 3** illustrates the standard process for IOL selection in the clinic.

1.4. State of the Art in Intraocular Lens Selection

With the overwhelming number of IOL designs available, choosing the correct IOL for a patient is not an easy task. Yet there are no reliable, objective tools that can help clinicians make this decision.

Decision tree algorithms have been proposed to guide the most appropriate surgery type for a given patient, but the scope is generally restricted to presbyopia surgery. For example, the degree of transparency of the crystalline lens will dictate whether to preserve the natural crystalline lens (and opt for a corneal presbyopic treatment or for a crystalline-lens-preserving IOL or phakic IOL) or whether a refractive lens exchange is more suitable, in which the natural lens is removed and replaced with an IOL, as in cataract surgery (56). However, the critical question of which lens is the most suitable for the patient remains out of reach with these algorithms.

The protocol of some clinicians includes fitting the patient with contact lenses (A. Cummings, personal communication), attempting to replicate different treatment principles. For example, clinicians may test for monovision (applying a monofocal contact lens for far vision in the dominant eye, and a monofocal corrected lens for near vision in the contralateral eye) or for multifocal contact lenses. A major drawback of using multifocal contact lenses as a simulation of postoperative vision with IOLs, besides confounding comfort factors associated with contact lens wear, particularly in nonhabitual contact lens wearers, is that multifocal contact lenses (which generally show refractive zonal designs) fail to represent the specific designs of multifocal IOLs (which are generally diffractive).

Alternatively, a crude way to represent what vision may look like with IOLs is to show the patient the simulated effects on images presented on a screen. The blurring or corrective effect of an optical correction can be simulated using Fourier optics. Thus, knowing the aberration map (phase map) that defines a certain correction, and therefore how a point source is imaged through an IOL (point spread function), a surgeon can simulate the blurring of any image by means of a convolution operation (19, 57). Although computational simulations are frequently used to illustrate the image quality provided by a lens at different foci with multifocal IOLs (similar to the experimental images obtained with optical benches that are used to characterize lenses), simulating visual performance by giving these images to patients is very limited, as it disregards the interactions of IOL optics with the patient's ocular aberrations. Some works attempt to reduce the effect of the eye's optics by using small artificial pupils that limit the contribution of

the patient's aberrations, which in turn are considered in the convolution process. The need for adapted calculations for each subject and the limitation of simulated conditions have prevented the clinical advancement of this type of simulation.

A turning point in simulations of optical corrections was the transfer of adaptive optics (AO) technology, originally developed to measure and compensate for the effects of atmospheric turbulence in astronomical observations through ground-based telescopes, to applications in the eye. The phase map describing the IOL can be mapped onto the AO active element (e.g., a deformable mirror or a spatial light modulator), which is then projected onto the patient's eye, mimicking the implantation of the IOL. Laboratory AO systems, and other alternatives to programmable corrections (such as those created with the concept of temporal multiplexing using optotunable lenses, e.g., SimVis), hold promise to become routine simulating technologies in the clinic by which patients can experience prospective postoperative vision with different IOL designs (58).

Adaptive optics (AO): technique derived from astronomy that manipulates the optical aberrations of the eye and mapping of lens designs

Anterior segment OCT: interferometric imaging technique allowing high-resolution tomographic imaging of the anterior portion of the eye in three dimensions

2. CUSTOMIZING INTRAOCULAR LENS SELECTION TO THE PATIENT'S EYE ANATOMY: ADDING THE CRYSTALLINE LENS TO THE EQUATION

2.1. Imaging the Crystalline Lens and Its Opacities

Cataracts are opacifications inside the crystalline lens. Diagnostic methods to determine the level of transparency loss and reduction of the contrast in the retinal image are important for deciding whether and when to perform a cataract procedure. Methods for detecting and evaluating cataracts include imaging-based techniques and stray-light measurement approaches. The first group utilizes images of the crystalline lens acquired by different technologies. Current clinical evaluation of lenticular opacities is based mostly on eye examination using slit-lamp microscopy. The subjective analysis of slit-lamp images of the lens is a basis for the cataract classification systems (e.g., Lens Opacification Classification System III) (59). Some alternatives in the second group measure the degradation of the retinal image quality produced by scatter. This can be achieved by recording double-pass retinal images (60) and quantifying the impact of the cataracts (61, 62).

A direct approach to measuring lens opacities involves imaging the crystalline lens in three dimensions by means of optical coherence tomography (OCT) technology. In particular, a long-range swept-source OCT utilizing short-wavelength external cavity tunable laser technology for in vivo 3D imaging of the crystalline lens has been presented to detect opacifications (63–65). Anterior segment OCT images of patients with cataract (**Figure 4**) were acquired with a high-speed swept-source OCT instrument operating at 1,050 nm for long-range imaging optimized for full anterior segment visualization, at an axial scan rate of 50 kHz and with a depth range of 17 mm, producing volumetric data sets consisting of 350 × 350 A-scans and covering 7 × 7 mm^2. Scattering is spatially resolved and can be visualized in three dimensions (**Figure 4*a–d*, subpanel *ii***) or through spatial depth projection intensities (**Figure 4*a–d*, subpanels *iii*, *iv***). The highly spatially resolved opacity distribution (cortical or nuclear), the opacity dimensions, and the scattering intensity allow a more detailed diagnostic and grading of cataract in patients.

2.2. Full 3D Crystalline Lens Geometry from Optical Coherence Tomography: Estimating the Intraocular Lens Position

Knowing the full shape of the crystalline lens is essential to the customization of emerging solutions for presbyopia and cataract. For proper sizing and customized design of accommodative IOLs (A-IOLs), prior knowledge of the full shape of the crystalline lens (and thus its diameter and volume) could be critical to the correct performance of the A-IOL and could enhance the

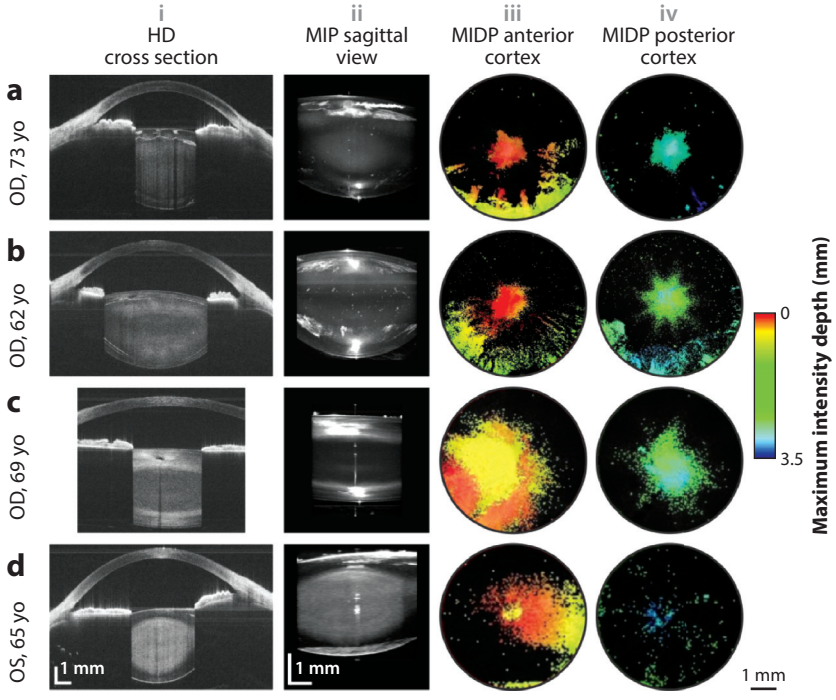

Figure 4

OCT imaging of crystalline lens opacities. SS-OCT imaging of cortical and nuclear cataract in the lens. (*a*) Cortical and nuclear cataract. (*b*,*c*) Cortical cataracts. (*d*) Nuclear cataract. (*i*) HD cross-sectional image. (*ii*) MIP (sagittal view). (*iii*) MIDP overlaid with the maximum intensity map for the anterior cortex. (*iv*) MIDP overlaid with the maximum intensity map for the posterior cortex. Figure adapted with permission from Reference 64 and the Optical Society of America. Abbreviations: HD, high density; MIDP, maximum intensity depth projection; MIP, maximum intensity projection; OD, right eye; OS, left eye; SS-OCT, swept source–optical coherence tomography.

refractive predictability (37, 66, 67). In cataract surgery, knowing the full shape of the crystalline lens improves the accuracy of estimating the ELP (i.e., where the IOL will fall axially in the eye once it is implanted) (68). Proper ELP estimation is critical to the selection of IOL power and thus the achieved refraction correction accuracy. According to Norrby (23), errors in ELP estimation, postoperative refraction, and axial length measurement by standard methods contribute to an average mean absolute error of 0.6 D. With current technologies this error can decrease to 0.4 D, although with future technologies this could decrease to 0.25 D, almost the barely noticeable refractive error.

The crystalline lens lies behind the cornea and the iris, and quantifying it is challenging. Optical techniques such as Purkinje imaging (69) and Scheimpflug imaging (70–73) have been used to assess some geometric aspects of the crystalline lens in vivo. But to obtain accurate estimates of the lens shape, optical imaging methods must correct optical distortion produced by refraction by the cornea and anterior lens surfaces. Nevertheless, any optical imaging technique of the anterior segment retrieves information visible only through the pupil, as the incident light is blocked by the iris, preventing the imaging of the peripheral zone of the crystalline lens.

Non-optical techniques such as magnetic resonance imaging (74, 75) or ultrasound biomicroscopy (76) visualize the full shape of the lens, including the peripheral region, although these

techniques generally present much lower resolutions and longer acquisition times and/or contact and suffer from other types of distortion.

Anterior segment 3D OCT combined with optical distortion correction algorithms (77) is an excellent technique to quantify the anterior segment of the eye, including the part of the crystalline lens visible through the eye's natural pupil (65, 78–84). Furthermore, we have recently proposed and validated methods to accurately estimate the full shape of the lens from its visible part (81, 85). Basically, a set of ex vivo lenses in which the entire crystalline lens is visible (because the iris is removed before the images are captured) were measured by a 3D-OCT system. In vivo conditions were simulated in the 3D ex vivo volumes, assuming that the information within only a given pupil size was available. The entire lens shape was estimated from the limited information on the pupil by a parametric model and then compared with the shape computed from the whole lens. The proposed method demonstrates improved performance compared with state-of-the-art methods, leading to volume, diameter, and equatorial plane position estimation errors approximately three, six, and four times lower on average, respectively (81).

We proposed a formula to estimate the postoperative IOL position from preoperative geometric parameters of the full shape of the lens (specifically, the position of the equator and the volume of the lens) (68). Simulations of different approaches to ELP estimation for the same eyes allowed us to compare the ELP estimation errors of the new method with those of the state-of-the-art methods. The mean ELP estimation error obtained by the proposed method was two and three times lower than that obtained with the C-constant by the Olsen formula (86) and with the standard SRK/T formula (47), respectively. Furthermore, to evaluate the improvements in terms of postoperative refraction estimation, researchers compared in retrospect the actual measured postoperative refraction with the simulated (predicted) refraction obtained with the SRK/T IOL power calculation formula, using the actual IOL power implanted and the different estimations of the IOL position. These simulations showed that, following the same selection criteria by the same surgeon, the proposed approach would have preoperatively selected a different IOL for approximately 40% of the eyes. **Figure 5** illustrates the quantification of the full crystalline lens geometry and the calculation of the ELP prediction formula.

2.3. New Intraocular Lens Power Estimations Using 3D Optical Coherence Tomography

As discussed in Section 2.2, calculation of IOL power and prediction of the lens position are crucial for attaining an optimal postoperative refractive outcome. However, the ELP is not a physical quantity that can be directly measured; rather, it is reversely calculated as an imaginary distance between the cornea and the principal plane of the IOL. This variable is necessary to estimate the actual postoperative refraction on the basis of available ocular biometry data. As described above, various statistical regression models formulated on the basis of preoperative measurements of ocular biometry have been proposed and used to reliably predict ELP before surgery. Currently, crystalline lens geometry is regarded as an essential element in newly developed formulas for calculating IOL power, such as the Olsen formula using the C-constant (86, 87), which uses preoperative ACD and LT, and the new Shammas formula (88), which uses ante-nucleus distance and nuclear thickness. Although these formulas produce acceptable estimates of postoperative IOL position, ACD and LT alone may have limited capacity to predict the postoperative IOL position. To overcome this limitation, researchers have proposed a new hypothesis that the IOL would most likely be stabilized in its position adjacent to the lens equator.

Presently, no commercial device is capable of imaging and evaluating the crystalline lens biometry completely in vivo and at high resolution, and ultrasound biomicroscopy and magnetic resonance imaging provide relatively poor image resolution and are challenging to utilize in clinical

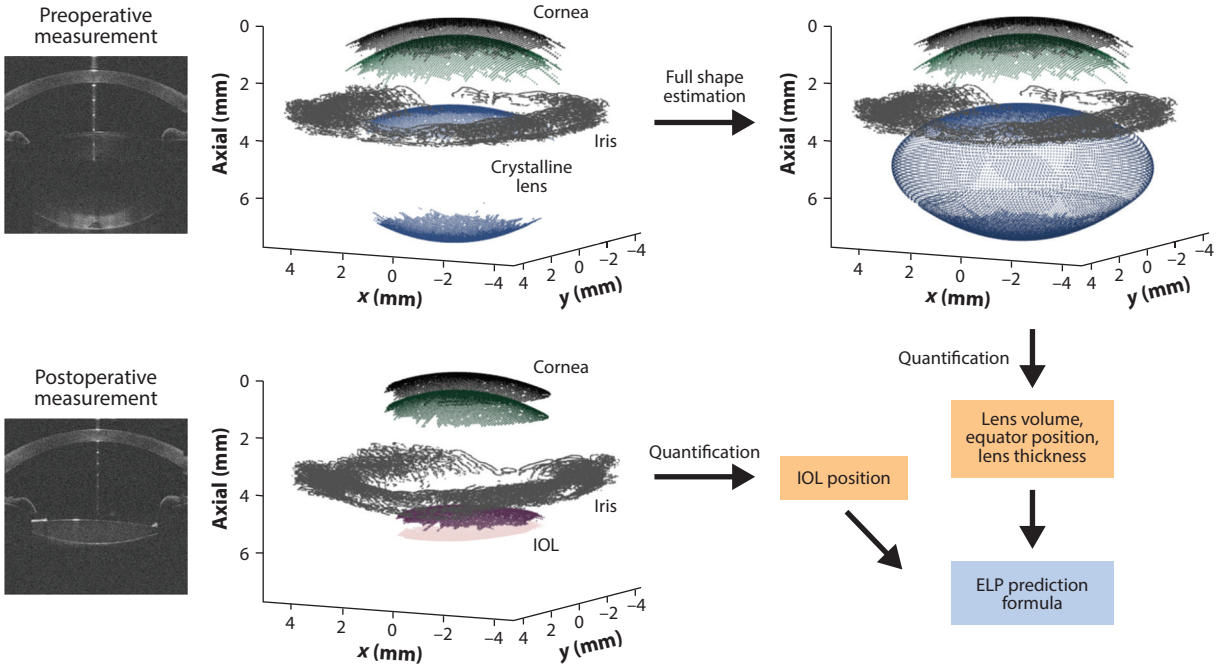

Figure 5

Quantification of the full crystalline lens geometry. OCT raw images of the ELP from preoperative and postoperative measurements are used to construct 3D models (81). The full shape of the crystalline lens is estimated from the central part visible through the pupil. The ELP prediction formula is obtained from the geometric parameters of the full shape of the preoperative crystalline lens and the postoperative IOL position. Abbreviations: ELP, estimated lens position; IOL, intraocular lens; OCT, optical coherence tomography.

settings (89). OCT is the highest-resolution noninvasive imaging technology that grants in vivo anterior segment biometry of the human eye. Recent advances in OCT-based anterior segment imaging make it possible to achieve high-quality visualization of the anterior segment from the cornea to the back surface of the crystalline lens (63, 68), and all future methods for ELP estimation point toward OCT as the technique of choice for the most complete quantification of crystalline lens geometry. In fact, as described in Section 2.2, laboratory OCT systems, novel image processing methods, and a priori knowledge of crystalline lens shape from an ex vivo data set have been used to estimate the full shape of the lens from OCT images of patients. Alternative methods, using commercially available OCT systems and a simpler extrapolation technique to determine the crystalline lens equator, have been combined with standard regression methods for analyzing many eyes in order to improve current ELP estimations and to propose a new IOL power estimation formula that incorporates additional crystalline lens parameters.

The Catalys Precision Laser System, one of the first clinically available femtosecond laser-assisted cataract surgery systems, is equipped with 3D OCT and provides axial and lateral resolutions of 30 and 15 μm, respectively. This imaging capability enables surgeons to measure parameters relevant to crystalline lens geometry, including LT and lens meridian parameter (LMP). LMP in particular is of great interest and is defined as the axial distance from the corneal apex to the equatorial plane of the crystalline lens. It is important to note that this OCT system cannot visualize the entire crystalline lens equator because the periphery of the crystalline lens is concealed behind the iris, although the application of techniques such as those described in Section 2.2 would enable this extrapolation. Simpler, embedded software can extrapolate the

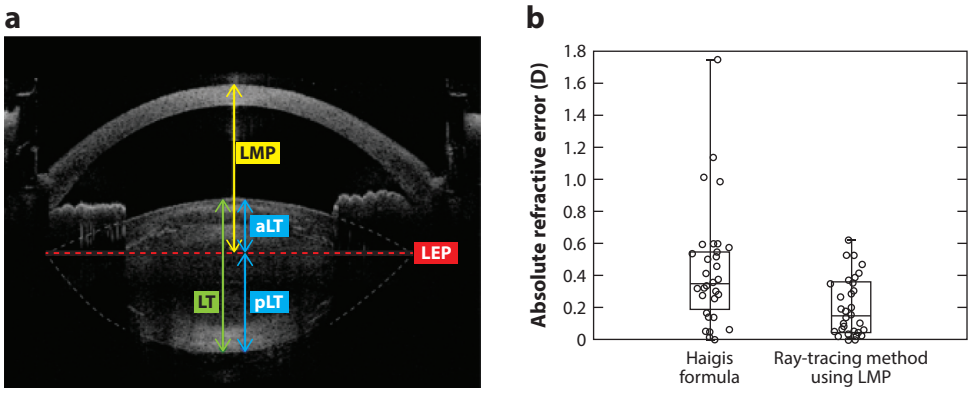

Figure 6

Toward new (OCT-based) formulas. (*a*) Anterior segment biometric measurements by 3D OCT. 3D OCT presents the entire capsule surface, which includes an extrapolated boundary (*gray dashed line*) demarcating the crystalline lens extended from the partially visualized anterior and posterior capsules, supported by the embedded software of the laser system. The LEP connects both ends of the anterior and posterior capsules. The LMP is the axial distance from the corneal apex to the equatorial plane of the crystalline lens. The total crystalline LT consists of two parts, aLT and pLT, divided by the equatorial plane. (*b*) Absolute prediction error for the ray-tracing method based on LMP and for clinical outcomes in the group of cataract patients in whom an IOL was implanted (CT Asphina, Zeiss, Jena, Germany). Median, quartile, minimum, and maximum values for absolute prediction error in each group are displayed on these plots. Figure adapted with permission from Reference 93 and the American Academy of Ophthalmology. Abbreviations: 3D OCT, three-dimensional optical coherence tomography; aLT, anterior lens thickness; LEP, lens equatorial plane; LMP, lens meridian parameter; LT, lens thickness; pLT, posterior lens thickness.

imaged interface of the anterior and posterior capsule surfaces to the point where the two extended surfaces intersect each other. This additional image processing estimates the lens equatorial plane connecting the two intersection points. Additionally, 3D OCT can measure other ocular biometry, including ACD, the thickness of the anterior part of crystalline lens (aLT), and the thickness of the posterior part of crystalline lens (pLT), as illustrated in **Figure 6*a***.

Using this system, Yoo et al. (90) reported that LMP was a vital parameter of preoperative crystalline lens geometry and a precise predictor of postoperative IOL position. Their study showed that median absolute errors calculated from the ray-tracing method using LMP were smaller than those from the Haigis formula, a frequently used open-source formula (91), as shown in **Figure 6*b***. In a follow-up study, Yoo et al. (92) also proposed that ACD, aLT, and pLT showed significant discrepancies between two subgroups classified according to LT: a thin lens group (LT $<$ 4.5 mm) and a thick lens group (LT $\geq$ 4.5 mm). Using this 3D-OCT-based segmentation method, the authors found that a formula combining axial length (AL), LMP, and pLT (ELP $= 1.143 + 0.148 \times$ AL $+ 0.428 \times$ LMP $+ 0.254 \times$ pLT) demonstrated a higher predictability for both ELP and refractive outcomes (93) than did existing IOL formulas, although further studies of a larger group of patients are required to validate these findings.

Despite the significant improvements in our capability to predict the IOL position after cataract surgery, significant intersubject variability still exists. This variability can be further reduced by implementing new variables from objective ocular imaging into more sophisticated regression analysis. However, the ultimate solution to this limitation is to develop a method for choosing the optimal IOL that is customized to an individual patient's ocular biometry and optical and mechanical properties.

2.4. Ray-Tracing Selection of Intraocular Lenses

Wave aberrations: optical phase distortions (relative to a perfect wavefront) accounting for the optical quality of a lens (or the eye)

Ray tracing: virtual (or experimental) evaluation of the optical quality based on the pathway of rays through a lens; also used in lens design

Fully anatomical computer eye models of pseudophakic eyes (implanted with IOLs) incorporating anterior and posterior corneal topography, IOL geometry, IOL tilt and decentration, eye rotation, and axial biometry (ACD and axial length) reproduce with great accuracy the wave aberrations measured in the same eyes by aberrometry techniques (82, 94–96) (**Figure 7*a–c***). Simulated wave aberrations (obtained by virtual ray tracing on custom computer eye models) have been compared with wave aberrations measured with a Shack-Hartmann wavefront sensor (94) or by laser ray tracing (82, 95, 96). Computer eye models are constructed with geometric information obtained from corneal videokeratoscopy, Scheimpflug (73) or Purkinje (94, 95) imaging, and more recently, fully quantitative 3D OCT (82, 96). 3D-OCT-based computer eye models can be constructed with information obtained with the same imaging instrument. The similarity between the simulated wave aberrations based on ray tracing on these computer eye models and the measured wave aberrations demonstrates that custom eye models represent excellent platforms to predict optical performance of a given IOL design in the particular eye of a patient and to test out different IOL options (virtual surgery/surgery planning) prior to the actual surgery (**Figure 7*d–g***).

Ray-tracing methods for selecting IOL power have also been proposed as an alternative to traditional IOL power formulas. By ray tracing, the IOL that produces the best focus in the retinal plane is selected. This approach relies on improved, accurate estimates of the postoperative lens position (as described in Sections 2.2 and 2.3), on accurate biometry, and on knowledge of the individual anterior and posterior corneal topography and IOL geometry. In turn, ray tracing considers specific interactions between the IOL and the ocular components, which are often missed using paraxial optics.

The traditional IOL power formulas described in Section 1.4 are based on paraxial equations, and efforts have generally attempted to increase the accuracy of the ELP. However, the optical quality depends also on the total higher-order aberrations, which occur for larger pupils and are unaccounted for when using paraxial optics. For instance, the positive spherical aberration of the cornea can vary between patients because of intersubject variability in corneal geometry or previous corneal surgery (97). While some IOLs are designed to compensate for the spherical aberration of the cornea, others overcompensate this aberration with the aim of extending the depth of focus. The optical quality of an eye with a given IOL can be calculated either by simulating the retinal image (98) or by calculating optical metrics associated with the wavefront aberrations or the modulation transfer function (MTF) (i.e., the loss of contrast of each spatial frequency in the retinal image) of the optical system. The area under the MTF was proposed as a method to estimate the best IOL for a given patient (99), and metrics such as the MTF weighted with the average human contrast sensitivity (CS) function correlated well with the through-focus visual acuity (VA) (100). OCT imaging devices are excellent tools for measuring not only the topography of the cornea (101) but also the IOL 3D position (102) and its tilt and decentration (102–104). A complete anatomical eye model can therefore be built with this information and simulate the prospective performance of different IOL designs by calculating the retinal image quality at best focus and at different distances. Simulations can be further refined by incorporating expected incision-induced changes in corneal geometry (105). Ray-tracing techniques on 3D pseudophakic eye models fully customized to the patient anatomy, including accurate estimations of the ELP based on information on the preoperative full crystalline lens geometry, which allow high fidelity in the simulation and optimization of the retinal image quality on the patient's eye, represent to date the best strategy for IOL selection for presbyopic and cataract surgery purely on the basis of optical grounds (106).

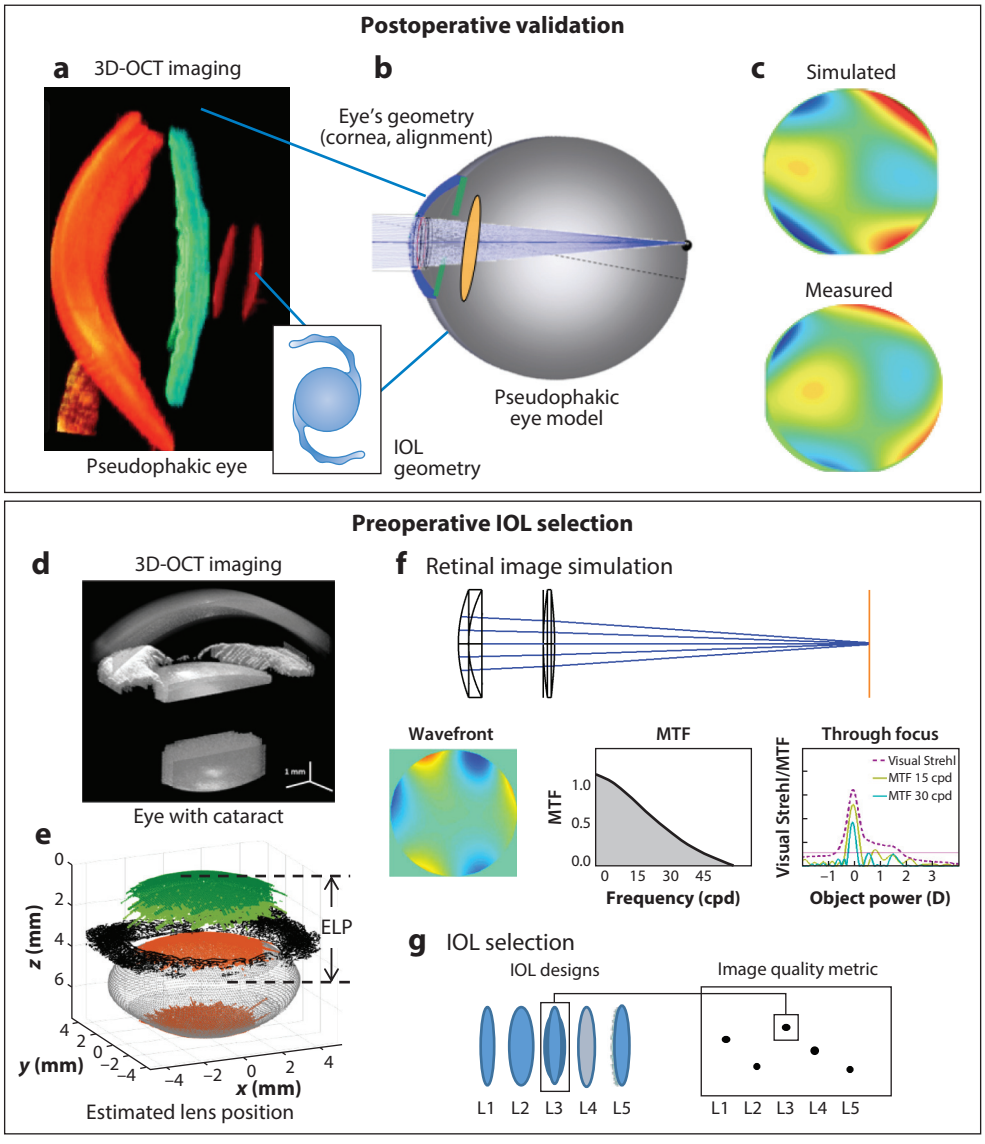

Figure 7

Optical simulations of IOL implantation. Custom model eyes based on full 3D anatomical information on the patient's eye have been validated postoperatively and can be used as a platform for selecting IOLs preoperatively. (*a*) Quantitative 3D-OCT image of a patient implanted with an IOL (102). (*b*) Corresponding custom model eye for the same patient (constructed using methods similar to those in Reference 69). (*c*) Simulated wave aberration (optical quality map at the pupil plane) from ray tracing on the custom model eye highly matches the measured wave aberration (through laser ray-tracing aberrometry) in the same eye (82), validating the model. (*d*) Volumetric image of the anterior segment of the eye captured by 3D OCT. Only the surfaces visible through the iris can be visualized but the full geometry can be estimated to calculate the ELP with custom-made methods (81). (*e*) Custom computer eye model based on a patient's anatomical data will allow the optics of the postsurgery eye to be characterized. (*f,g*) Different IOL designs can be evaluated, and the design that maximizes a selected quality metric is chosen before the surgery. Abbreviations: 3D OCT, three-dimensional optical coherence tomography; cpd, cycles per degree; ELP, effective lens position; IOL, intraocular lens; MTF, modulation transfer function.

3. CUSTOMIZING INTRAOCULAR LENS SELECTION TO THE PATIENT'S VISUAL PREFERENCE: THE ROLE OF VISUAL SIMULATORS

3.1. Adaptive Optics and Selection of Intraocular Lenses

As described in Section 2, the selection of IOLs can be optimized to fit some properties of the patient's eye geometry. In standard clinical practice, the customization is currently limited to the power of the lens. Although selection of the lens type (**Figure 2**) could be based on optical simulations of the through-focus retinal image quality, in practice, recommendations by the surgeon are based on their idea of the patient's visual expectations. Even optical simulations cannot capture all the visual aspects upon which tolerance of a certain lens type depends.

AO visual simulators offer the technology to overcome the limitations of current approaches by allowing patients to experience a prospective IOL before implantation. AO technology for visual testing has been developed and demonstrated in experimental laboratories and has even been made available in the clinic (58). A prime example of this technique has been developed by LOUM (Laboratorio de Optica de la Universidad de Murcia, Spain) and its spin-off company, Voptica (107–115).

Common elements of all AO systems include a wavefront sensor to measure the eye's aberrations and an active correcting device (**Figure 8*a***). Generally, a Shack-Hartmann wavefront sensor operating in IR light measures the eye's aberrations and residual defocus in real time. In the second pass, after the light is reflected in the retina and passes through the complete system, an array of lenslets, optically conjugated with the subject's pupil plane, produce an image of spots on a camera. The locations of the spots provide the local slopes of the ocular wavefront aberration. The correcting/manipulating device is placed in the system conjugated with both the subject's pupil plane and the wavefront sensor by using appropriate sets of lenses in a telescope configuration. In the LOUM device the active element is a spatial light modulator (a liquid crystal on silicon; **Figure 8*b***) onto which the optical corrections are mapped. Subjects view a stimulus (letters or any visual scene) displayed on a microdisplay. **Figure 8*c*** presents the VAO clinical instrument by Voptica and a diagram of the LOUM laboratory system (112).

AO instruments have been used to help design new types of IOLs (111, 116). However, making visual simulations clinically available has allowed the correction to be customized to the patient's needs and tolerances. For example, the VAO instrument has demonstrated the potential to customize corneal refractive surgery (117) and the relation between tolerance for spherical aberrations and certain systemic diseases (118).

A recent study has used the VAO instrument to fine-tune the spherical aberration of EDOF IOLs in a group of patients (119). Induction of spherical aberration (−0.15 and −0.30 μm over 4.5-mm pupils) decreased VA significantly at far but improved it at near as the magnitude of negative spherical aberration increased, although through-focus performance varied across the 17 subjects in the study (**Figure 8*f***). An optimum solution for through-focus performance (fulfilling a certain VA threshold) as a combination of spherical aberration and focus shift could be found for each patient, indicating the suitability of visual simulators for customizing a visual correction.

3.2. Adaptive Optics and Strategies to Improve Through-Focus Performance to Correct Presbyopia

Progress in the accurate measurement and correction of the eye's aberration through AO has provided an opportunity to apply wavefront technology to clinical problems to ameliorate visual performance (58, 120). By correcting higher-order aberrations beyond conventional

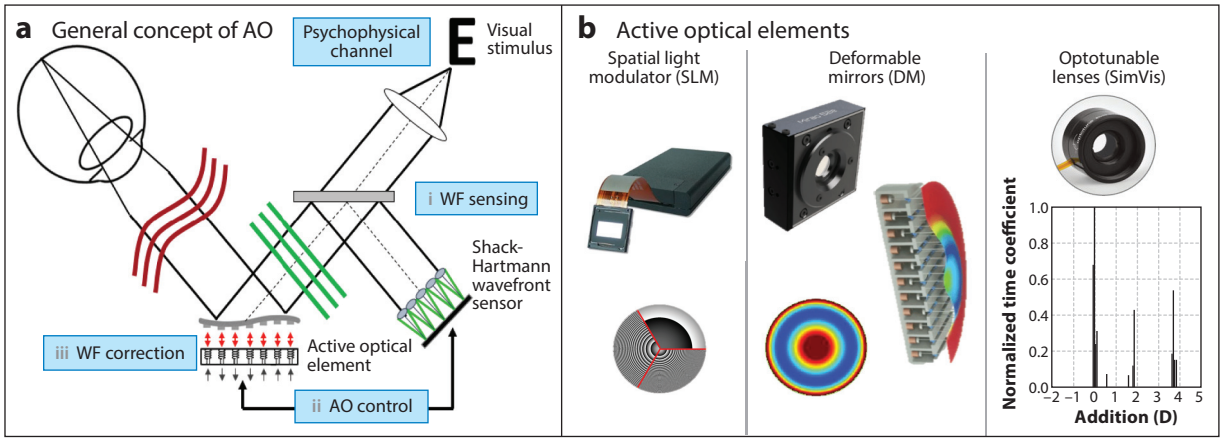

AO visual simulators

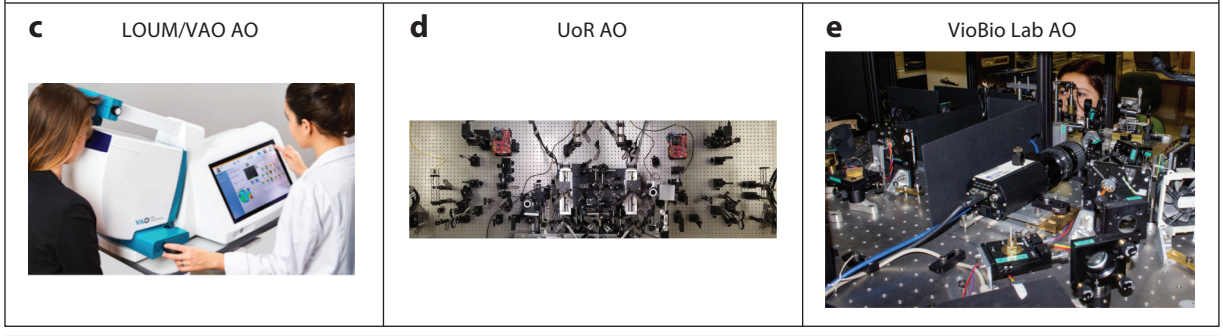

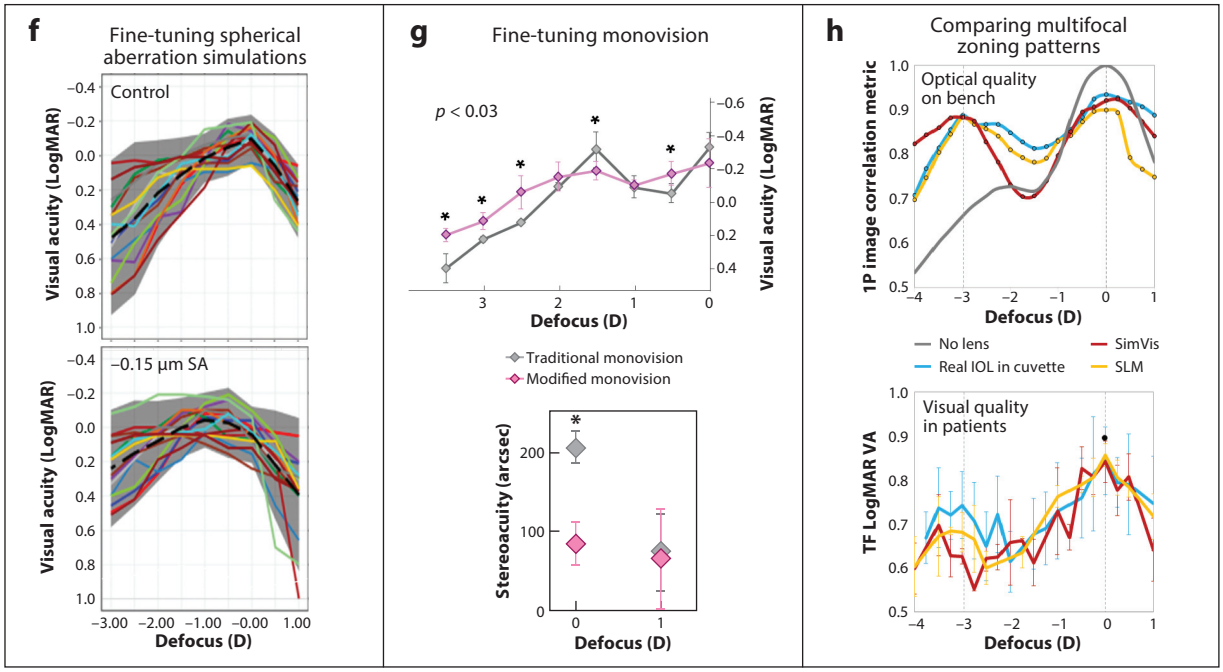

(*Caption appears on following page*)

Figure 8 (*Figure appears on preceding page*)

AO simulators. (*a*) General concept for AO visual simulators containing a Shack-Hartmann wavefront sensor that measures aberrations and an active element that corrects and/or induces aberrations or a certain phase map representing an optical correction (i.e., an IOL). (*b*) The active element can be (*left*) an SLM (LOUM AO, Voptica VAO, and VioBio AO systems), (*middle*) a DM (by Alpao of the UoR AO system and by Imagine Eyes of the VioBio AO system), or (*right*) an optotunable lens working under temporal multiplexing (SimVis of the VioBio AO system and SimVis Gekko by 2EyesVision). (*c*) A VAO system and (*f*) through-focus visual acuity through a spherical aberration of 0 (*top*) or −0.15 μm (*bottom*) mapped onto the SLM in 17 subjects with paralyzed accommodation obtained with VAO. Panels *c* and *f* are as described in Reference 119. (*d*) The UoR binocular AO system and (*g*) an example of improvement in (*top*) near visual acuity and (*bottom*) stereovision with modified monovision (fine-tuning spherical aberration in the nondominant eye in one patient) obtained with that instrument. Panels *d* and *g* are as described in Reference 126. (*e*) The VioBio AO system and (*h*, *top*) through-focus optical performance with a bifocal lens, a lens inserted into a cuvette, a lens mapped onto the SLM or mapped on the SimVis, and a lens in an artificial eye. (*Bottom*) Visual performance in a patient with paralyzed accommodation. Panels *e* and *h* are as described in Reference 44. Abbreviations: AO, adaptive optics; DM, deformable mirror; IOL, intraocular lens; LOUM, Laboratorio de Optica de la Universidad de Murcia; SA, stereoacuity; SLM, spatial light modulator; TF, through-focus; UoR, University of Rochester; VioBio, Visual Optics and Biophotonics Lab; WF, wavefront.

sphero-cylindrical refraction, AO improves human visual performance such as CS, VA, and real-life tasks (121–124). Most studies of optical compensation of higher-order aberrations are restricted to monocular vision; however, binocular visual functions help us understand how visual inputs from the two monocular channels are combined by the brain (112, 125). By manipulating the ocular aberrations, a binocular AO vision simulator is a powerful tool to advance our knowledge of the impact of the eyes' optics on neural processing and visual perception.

The binocular AO vision simulator developed at the University of Rochester (UoR) (Rochester, New York) consists of two identical monocular AO systems (**Figure 8*d***). Each monocular AO system is composed of a custom-made Shack-Hartmann wavefront sensor to measure the eye's wavefront aberration, a large-stroke deformable mirror with 97 actuators (Alpao) to control subjects' aberrations (**Figure 8*b***), a Badal optometer to vary object distance for through-focus vision testing, motorized vergence control, binocular fusion locks, an artificial pupil to simulate effective pupil sizes, and a visual stimulus channel with a digital display. The system uses an IR superluminescent diode for wavefront sensing and control, and vision testing is done under spectral conditions ranging from monochromatic to white light. The AO control can correct the eye's aberrations to make the eye diffraction limited in real time (up to 30 Hz) while the subject's visual performance is being measured. Different visual tasks, including VA, contrast sensitivity function, stereopsis, virtual reality, and motion perception, can be tested on a wide visual field (up to 4.7 × 8.4 deg), and values of spherical aberrations in the dominant eye that optimize visual performance at near and stereopsis can be found (126) (**Figure 8*g***).

AO instruments can also produce an arbitrary aberration profile of the eye. As indicated above, one application of this function is presbyopia correction in which various optical profiles that increase depth of focus can be simulated to evaluate through-focus visual performance from far to near. In addition to the described IOLs based on refractive and diffractive multifocal optical designs and EDOF lenses (**Figure 2**), other strategies can be tested using AO to reduce photic phenomena associated with these corrections, such as halos and glare (127), which can cause significant visual discomfort to patients, particularly in a lower light level. A previous study (128) proposed that apodization of light transmission in the pupil could reduce this problem, increasing visual benefit of presbyopia correction with spherical aberration through focus. The pupil apodization does not induce phase rectification, but it does enhance through-focus retinal image quality by shifting the phase reversals in the optical transfer function to higher spatial frequencies.

Monovision has been a popular clinical approach to overcoming presbyopia. Traditional monovision induces anisometropia, for which the nondominant eye is corrected for near vision and

the dominant eye is corrected for distant vision. Nonetheless, differences in interocular defocus of more than 2.0 D can reduce intermediate VA and CS (129); moreover, significant interocular differences in optical quality impair depth perception (130). To overcome these limitations, researchers proposed modified monovision in which the interocular difference is reduced by extending depth of focus in one or both eyes. Using the binocular AO vision simulator described above, Zheleznyak et al. (131) reported that modified monovision with spherical aberration leads to a significant benefit in binocular depth of focus and VA compared with traditional monovision. The top graph in **Figure 8*g*** demonstrates the improvement when comparing through-focus binocular visual performance, under which the traditional monovision was simulated with 1.5 D anisometropia and the modified monovision was achieved with a spherical aberration of +0.1 and −0.4 μm in the dominant and nondominant eyes, respectively. Although this enhancement was obtained at the expense of slight CS degradation at the anisometropic position, the reduced interocular difference in through-focus image quality improved binocular summation and high-contrast VA. Furthermore, stereoacuity at far with modified monovision was significantly improved compared with stereoacuity at far with traditional monovision (see the bottom graph in **Figure 8*g***).

The AO vision simulator equipped with a deformable mirror and a spatial light modulator enables us to control complicated phase and amplitude profiles of light and to investigate the impact of the optical manipulation on visual performance, providing practical and clinical guidelines for current and future vision correction techniques.

3.3. Adaptive Optics and Simultaneous Vision Simulators: Providing Patient's Preoperative Experience of Postoperative Vision

The active elements of the AO simulators presented in Section 3.1 (LOUM/VioBio) are spatial light modulators, and those of the AO simulators presented in Section 3.2 (UoR) are deformable mirrors (**Figure 8*b***). These elements are used either to correct the subject's aberrations or to reproduce the equivalent phase map of a certain optical design. The VioBio Lab AO Visual Simulator (**Figure 8*e***) is a multiple-channel system (58, 132–134). One channel comprises a deformable mirror (MIRAO, 52 actuators, Imagine Eyes) to correct for optical aberrations dynamically or to simulate lenses with smooth-varying profiles, another channel comprises a spatial light modulator to simulate zonal or diffractive lenses, another channel comprises a cuvette to insert a physical IOL, and another channel has optotunable lenses working in temporal multiplexing mode (Sim+Vis Technology™, or SimVis) (135, 136). SimVis allows fast periodic foci variations at speeds greater than the flicker fusion threshold of the human visual system, delivering seemingly static images on the subject's retina that emulate the effect of the multifocal correction (135, 137).

The availability of multiple channels allows cross-validation of the different simulating techniques, both optically on bench and visually in subjects (**Figure 8*b***). For example, we have shown that multifocal zonal (bifocal, trifocal, and tetrafocal) patterns represented in a spatial light modulator reproduce the optical quality of equivalent physical phase plates (133) (**Figure 8*e***). Furthermore, both spatial-light-modulating visual simulators and SimVis accurately captured through-focus optical quality and visual quality with zonal bifocal refractive and diffractive trifocal commercial IOLs (inserted into a cuvette and projected onto the patient's pupil) (44). Other studies have used visual simulators to investigate visual quality and visual perception with bifocal corrections of different near addition magnitudes (138) and different near and far zone distributions (139, 140).

An advantage of the SimVis technology is the possibility that it can be made into a compact system (wearable, 20° field-of-view, see-through, and binocular), allowing easy use in clinical practice. This clinical device (SimVis Gekko™, 2EyesVision, Spain) has already been demonstrated in

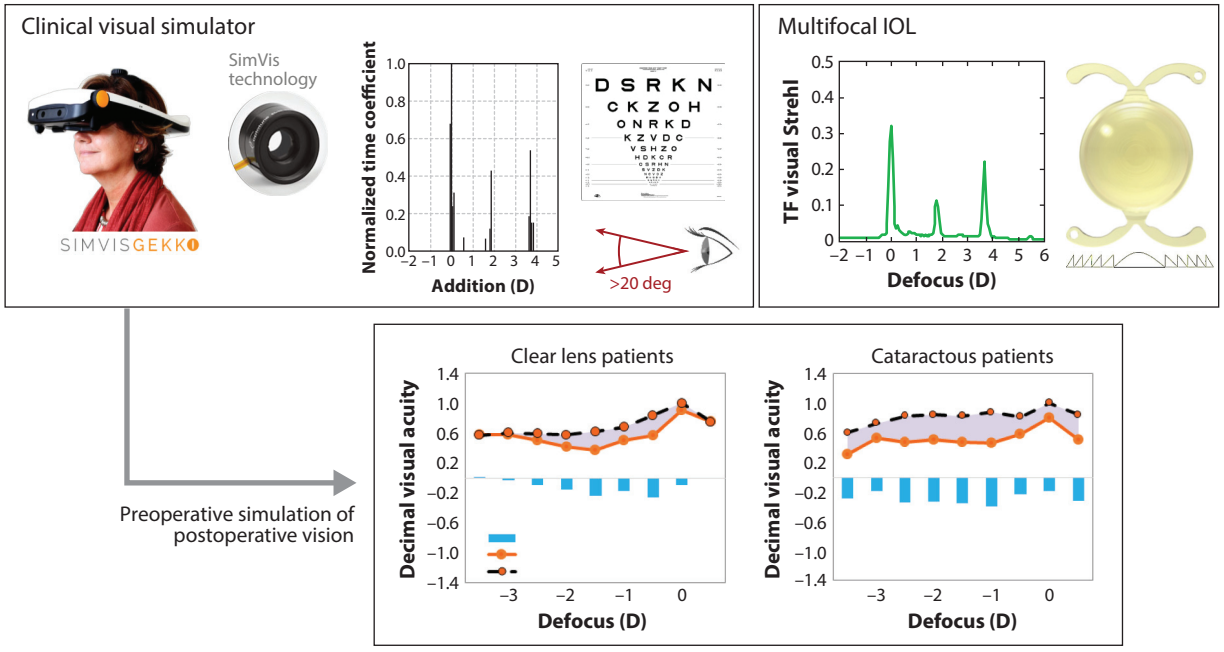

Figure 9

Preoperative visual simulations of post–cataract surgery vision. Through-focus visual acuity measured with trifocal diffractive IOLs simulated in the wearable binocular SimVis Gekko visual simulator before surgery compared with measurements using the implanted trifocal diffractive IOL after surgery. Insets show the temporal coefficients describing the IOL in SimVis and the through-focus performance of the simulated lens. Figure adapted with permission from Reference 141 and the American Academy of Ophthalmology. Abbreviations: D, diopter; IOL, intraocular lens.

patients. A study compared through-focus VA measured preoperatively, with the device simulating commercial trifocal diffractive IOLs (Finevision Pod F, PhysIOL, Belgium), and then postoperatively, with the implanted real IOL (141). The study was performed on eight presbyopic patients with clear crystalline lens ($n = 5$) or with crystalline lens with some degree of cataract ($n = 3$, N1 to N4) (**Figure 9**). There was a high equivalence in the relative through-focus VA curves pre- and postoperatively. Furthermore, the results suggest that, at least in patients with mild cataracts, a simple conversion factor would be needed to project the expected through-focus performance after cataract removal from preoperative simulation measurements. Visual simulators open up the possibility to try numerous correction options before surgery, including binocular corrections such as monovision or modified monovision (Section 3.2) or mix-and-match corrections (different multifocal corrections in both eyes). A recent study using binocular SimVis revealed different preferences across patients exposed to 17 different correction combinations of binocular corrections (monofocal, bifocal, and trifocal) (142), suggesting that visual simulations are highly valuable clinical tools for the personalized management of not only IOL implantation but also contact lens fitting (143), and even for exploring prospective neural adaptation to and perceptual learning aspects of a given correction (144, 145).

Multifocal correction: correction for presbyopia (with refractive or diffractive designs) based on the principle of simultaneous vision (i.e., projecting simultaneously images focused at far and at near)

4. FUTURE DIRECTIONS

We envision that future paradigms for IOL selection for cataract surgery will entail customization to the patient's eye anatomy and visual simulations to anticipate vision prior to surgery (**Figure 10**).

Figure 10

The future of postcataract vision simulation and IOL selection. 3D quantitative optical coherence tomography, providing complete biometric and geometric information, holds promise to become the technique of reference for selecting the optimal IOL power. Quantitative input data allow eye models to be constructed as platforms for testing, virtual surgical planning, and IOL selection, adjusted to the patient's anatomy. Visual simulators, which allow patients to visualize the visual outcomes of a surgery prior to implantation, hold promise to help surgeons make informed decisions about IOL selection and customize the selection to the patient's visual needs. Abbreviation: IOL, intraocular lens.

The technologies described above will overcome the challenges of present methods for cataract surgery, particularly those associated with choosing the most appropriate presbyopia treatment (corneal or lens exchange, which relies on correct assessment of lens opacity), selecting the correct IOL power, choosing the most appropriate lens design, and managing patient expectations. These goals are not without potential hurdles, which will be necessary to overcome, and new opportunities with which to leverage the prospective technologies described herein.

New 3D biometric technologies and new strategies for selecting IOL power need a change of clinical paradigm, as current methods have been established for decades. In addition to proper clinical studies demonstrating the superiority of the proposed methods, question arise about the most adequate route to deployment: Will the quantification routines be available in all commercial OCT devices? Will calculations be available in a cloud-based system where clinicians can upload OCT images or biometric data for simulation and IOL power calculations? Should this movement be led by OCT manufacturers and medical imaging device companies rather than by IOL manufacturers? How will proprietary IOL designs (ultimately necessary for IOL power calculations) be implanted in the ray-tracing models?

Although the described computer eye models are platforms for virtual planning of surgery based purely on optical simulations, they may be expanded to incorporate biomechanical

response. Those extensions can entail finite element modeling of the cornea [e.g., to predict the effect of corneal incisions through which IOLs are implanted (146) or to predict the change in corneal shape upon insertion of intracorneal implants (147)] or the effect of the capsular bag [e.g., on the compression of the haptics of the IOL (148), with a potential impact on ELP]. These optomechanical models would link a common surgery simulation platform with existing separate efforts of optical and mechanical modeling and would constitute the most comprehensive virtual surgical platform in ophthalmology existing to date.

The described technologies hold also great potential in research and development of new IOLs, prior to the manufacturing and surgical clinical trials. Using realistic computer eye models in both the design and the computational validation of the IOLs will likely result in higher-quality lenses and better-informed expectations of the optical performance of the lens in the patient's eye. In addition, replacing expensive clinical trials with clinical studies in which lenses are simulated with visual simulators, rather than implanted, will efficiently save resources and lead to a better comparative analysis (tested in the same eye) of different designs.

Standard practice for IOL implantation relies on stocks of lenses, which are designed in finite power steps (generally in 0.5 D). Some trends suggest future avenues not only for customized IOL selection but also for customized IOL design (149). For example, light-adjustable IOLs aim to intraoperatively fine-tune IOL power (by changing in situ the shape of the IOL by application of UV irradiation) (150). As 3D printing or other technologies for rapid production of optical-grade (and sterilized) IOLs may become available in the future (151), à la carte prescription of IOLs, specifically designed for a subject by applying optical design optimization techniques to custom computer eye models and visual simulations, can be envisioned.

Except in specific cases (i.e., pseudophakic IOLs receiving add-on lenses, phakic IOLs), IOLs are implanted after the crystalline lens is extracted, yet preoperative simulations are performed in the presence of the natural (in many cases, opacified) crystalline lens. Furthermore, the fact that the visual system recalibrates to new visual experiences cannot be overruled. Strategies to bypass the effect of the crystalline lens on the visual simulations (152), and to account for or anticipate the effect of visual adaptation (144), are needed.

As for optical simulations, dedicated visual simulations require knowledge of the commercial IOL optical designs that are programmed in the visual simulators to be demonstrated to patients. Making IOLs available for demonstration will be advantageous for IOL companies, clinicians, and patients, yet this requires partnerships between developers and IOL manufacturers, as well as efforts to incorporate visual simulation tests in the clinical protocol for IOL selection.

The described technologies are aimed at individualized preoperative assessment and customized surgical planning, yet other emerging new directions in IOL selection propose the use of artificial intelligence to produce new IOL formulas that consider complex relations between existing preoperative parameters (153). One may envision combining the power of comprehensive preoperative measurements and calculations with artificial intelligence and data science to unravel new relationships between geometric, optical, and visual parameters pre- and postoperatively and to select the best possible IOL for a patient.

Although some of the described technologies (instrumentation or premium IOLs) target patients in developed countries, where in many cases patients must pay for elective surgeries, cataract surgery to date continues to be out of reach for large fractions of the population in developing countries and remains the leading cause of blindness in some underserved areas. Increasing accessibility and reducing the cost and complexity of some of the optical instrumentation described here, such that cataract surgery is made more accurate, more safe, and more accessible, will greatly benefit health and society.

5. SUMMARY

Presbyopia and cataract result from age-related changes in the crystalline lens of the eye and affect billions of people worldwide. Replacement of the crystalline lens with an artificial intraocular lens (IOL) is the most frequently performed surgery in the world each year. An increasing number of presbyopic patients also receive IOLs (generally multifocal) with the aim of gaining functional vision at near and at far. With the aging of the world population, the health burden of these ocular conditions and the market size of IOLs are steadily increasing.

There are hundreds of different IOL designs and thus a growing selection of IOLs, making the choice of the most appropriate lens for a patient challenging. The increased complexity in lens design has not been in general paralleled by a sophistication in the information gathered preoperatively nor in the methods used in IOL selection.

Current methods for calculating IOL power use limited anatomical information about the patient (namely corneal power, obtained by keratometry, and axial length, obtained by ultrasound or optical low-coherence interferometry techniques). IOL power formulas are generally based on relations obtained from large data sets and empirical constants. Some formulas work better for longer or shorter eyes, while other formulas have been defined in patients who do not meet the original assumptions of geometric relations in the eye (e.g., post–corneal surgery patients).

3D optical coherence tomography (OCT) promises to become the technique of choice for preoperative assessment and quantification in cataract patients and prior to IOL implantation. Current swept-source OCT methods allow 3D imaging of cataract opacities, mapping the sources of preoperative image degradation by scattering. In particular, new OCT methods for quantifying the anterior segment OCT images, including corrections of scanning and optical distortions and extrapolation of the crystalline lens shape beyond the iris margin, allow 3D geometric and biometric data of anterior and posterior corneal topography, full crystalline lens geometry, interocular distances and misalignments, and most importantly, estimated lens position.

OCT-based pseudophakic computer eye models fully customized to the patient's anatomy accurately predict optical performance. Ray-tracing methods on these computer models can serve as platforms to simulate retinal image quality with different IOLs in the eye, and therefore may become the method for selection of both IOL design and IOL power that optimizes retinal image quality metrics.

Because the ultimate goal of IOL implantation is to provide the patient the best possible vision, it is important to adjust the IOL selection such that it meets the patient's visual needs and provides not only good retinal image quality but also functional and perceptually tolerated vision. Currently, this is achieved by surgeon–patient discussions and strategies for managing patient expectations. Some surgeons have patients try on contact lenses to simulate what the patient can expect from certain presbyopic solutions.

Adaptive optics technologies have been used in the laboratory to test vision through programmable corrections (typically mapped onto deformable mirrors or spatial light modulators). Wearable simulators (working under the principle of simultaneous vision) that allow binocular, see-through vision of the world through programmed lenses have also been released. Visual simulations therefore give patients the experience of vision with various IOLs prior to implantation. For effective application in clinical settings, technologies should be simultaneously accurate, easy to use, low cost, fast, and robust. To maximize the impact, these new technologies may ultimately need to be paired with innovative business models, strategic partnerships with IOL manufacturers, and deployment strategies.

DISCLOSURE STATEMENT

The following patents have a direct relationship (in whole or part) with the technologies described in this article: S.M., E.M.-E., and C.D. are inventors on US Patent US20170316571A1. S.M. and E.M.-E. are inventors on US Patent US20200268248A1. S.M. and C.D. are inventors on US Patents US9593933B2, US8876289B2, and US9693679B2. S.M., M.V., and C.D. have financial interest in 2EyesVision, Sociedad Limitada (SL). C.D. is an employee of 2EyesVision, a company that sells the SimVis visual simulator. G.Y. has financial interests in Ovitz, NextCorps, Johnson & Johnson, Bausch Health, and CooperVision. P.A. is an inventor on US Patents US8506079 and US891108 and is the chairman of Voptica, SL, a company that sells VAO, an adaptive optics simulator. The Visual Optics and Biophotonics Laboratory (S.M., E.M.-E., A.d.C., M.V.) receives research funding from the following IOL and contact lens manufacturers: PhysIOL-BVI, Johnson & Johnson, Alcon Research Labs, Alcon Research Institute, Hoya Surgical Optics, and CooperVision. The Advanced Physiological Optics Laboratory (G.Y. and S.P.) receives research funding from Johnson & Johnson, Bausch Health, and Clerio Vision.

ACKNOWLEDGMENTS

The authors have received funding from the following sources: H2020-MSCA-ITN-2015-675137 IMCUSTOMEYE (S.M.); ERC-2011-AdG-294099 PRESBYOPIA (S.M.); ERC-PoC-OCT4IOL (S.M.); ERC-PoC-SimVisSim (S.M.); ERC-2018-AdG-833106-SilkEye (S.M.) and ERC-2013-AdG-339228 SEECAT (P.A.); Spanish Agencia Estatal de Investigación FIS2017-84753-R (S.M.) and PID2019-105684RB-I00 (P.A.); Fundación Séneca-Agencia de Ciencia y Tecnología de la Región de Murcia 19897/GERM/15 (P.A.); National Institutes of Health/National Eye Institute (G.Y.); Research to Prevent Blindness (G.Y.); and NYSTAR/CEIS/CoE (G.Y.).

LITERATURE CITED

1. Glasser A, Campbell MC. 1998. Presbyopia and the optical changes in the human crystalline lens with age. *Vis. Res.* 38:209–29
2. McLellan JS, Marcos S, Burns SA. 2001. Age-related changes in monochromatic wave aberrations of the human eye. *Investig. Ophthalmol. Vis. Sci.* 42:1390–95
3. Artal P, Berrio E, Guirao A, Piers P. 2002. Contribution of the cornea and internal surfaces to the change of ocular aberrations with age. *J. Opt. Soc. Am. A Opt. Image Sci. Vis.* 19:137–43
4. de Castro A, Siedlecki D, Borja D, Uhlhorn S, Parel JM, et al. 2011. Age-dependent variation of the Gradient Index profile in human crystalline lenses. *J. Mod. Opt.* 58:1781–87
5. Birkenfeld J, de Castro A, Marcos S. 2014. Contribution of shape and gradient refractive index to the spherical aberration of isolated human lenses. *Investig. Ophthalmol. Vis. Sci.* 55:2599–607
6. Moreno-Barriuso E, Marcos S, Navarro R, Burns SA. 2001. Comparing laser ray tracing, the spatially resolved refractometer, and the Hartmann-Shack sensor to measure the ocular wave aberration. *Optom. Vis. Sci.* 78:152–56
7. Liu Y-C, Wilkins M, Kim T, Malyugin B, Mehta JS. 2017. Cataracts. *Lancet* 390:600–12
8. Holden BA, Fricke TR, Ho SM, Wong R, Schlenther G, et al. 2008. Global vision impairment due to uncorrected presbyopia. *Arch. Ophthalmol.* 126:1731–39
9. Glasser A. 2008. Restoration of accommodation: surgical options for correction of presbyopia. *Clin. Exp. Optom.* 91:279–95
10. Gil-Cazorla R, Shah S, Naroo SA. 2016. A review of the surgical options for the correction of presbyopia. *Br. J. Ophthalmol.* 100:62–70
11. Wolffsohn JS, Davies LN. 2019. Presbyopia: effectiveness of correction strategies. *Prog. Retin. Eye Res.* 68:124–43
12. Charman WN. 2014. Developments in the correction of presbyopia II: surgical approaches. *Ophthalmic Physiol. Opt.* 34:397–426

13. Rao GN, Khanna R, Payal A. 2011. The global burden of cataract. *Curr. Opin. Ophthalmol.* 22:4–9
14. Norregaard JC, Bernth-Petersen P, Alonso J, Andersen TF, Anderson GF. 2003. Visual functional outcomes of cataract surgery in the United States, Canada, Denmark, and Spain: report of the International Cataract Surgery Outcomes Study. *J. Cataract Refract. Surg.* 29:2135–42
15. Ibrahim M, Bhandari A, Sandhu JS, Balakrishnan P. 2006. Making sight affordable (part I): Aurolab Pioneers production of low-cost technology for cataract surgery. *Innov. Technol. Gov. Glob.* 1:25–41
16. Singh K, Misbah A, Saluja P, Singh AK. 2017. Review of manual small-incision cataract surgery. *Indian J. Ophthalmol.* 65:1281–88
17. IMARC Group. 2020. *Cataract Surgical Devices Market: Global Industry Trends, Share, Size, Growth, Opportunity and Forecast 2020–2025*. Rep., IMARC, Sheridan, WY
18. Zhang F. 2019. Femtosecond laser-assisted cataract surgery versus conventional cataract surgery comparison. *J. Cataract Refract. Surg.* 45:889
19. Marcos S, Barbero S, Jiménez-Alfaro I. 2005. Optical quality and depth-of-field of eyes implanted with spherical and aspheric intraocular lenses. *J. Refract. Surg.* 21:223–35
20. de Silva SR, Evans JR, Kirthi V, Ziaei M, Leyland M. 2016. Multifocal versus monofocal intraocular lenses after cataract extraction. *Cochrane Database Syst. Rev.* 12:CD003169
21. Alio JL, Plaza-Puche AB, Férnandez-Buenaga R, Pikkel J, Maldonado M. 2017. Multifocal intraocular lenses: an overview. *Surv. Ophthalmol.* 62:611–34
22. Hoffman RS, Fine IH, Packer M. 2003. Refractive lens exchange with a multifocal intraocular lens. *Curr. Opin. Ophthalmol.* 14:24–30
23. Norrby S. 2008. Sources of error in intraocular lens power calculation. *J. Cataract Refract. Surg.* 34:368–76
24. Drexler W, Findl O, Menapace R, Rainer G, Vass C, et al. 1998. Partial coherence interferometry: a novel approach to biometry in cataract surgery. *Am. J. Ophthalmol.* 126:524–34
25. Raymond S, Favilla I, Santamaria L. 2009. Comparing ultrasound biometry with partial coherence interferometry for intraocular lens power calculations: a randomized study. *Investig. Ophthalmol. Vis. Sci.* 50:2547–52
26. Tang M, Wang L, Koch DD, Li Y, Huang D. 2012. Intraocular lens power calculation after previous myopic laser vision correction based on corneal power measured by Fourier-domain optical coherence tomography. *J. Cataract Refract. Surg.* 38:589–94
27. Behndig A, Montan P, Stenevi U, Kugelberg M, Zetterström C, Lundström M. 2012. Aiming for emmetropia after cataract surgery: Swedish National Cataract Register study. *J. Cataract Refract. Surg.* 38:1181–86
28. Venter JA, Pelouskova M, Collins BM, Schallhorn SC, Hannan SJ. 2013. Visual outcomes and patient satisfaction in 9366 eyes using a refractive segmented multifocal intraocular lens. *J. Cataract Refract. Surg.* 39:1477–84
29. Woodward MA, Randleman JB, Stulting RD. 2009. Dissatisfaction after multifocal intraocular lens implantation. *J. Cataract Refract. Surg.* 35:992–97
30. Jones C. 2020. *United States Cataract Atlas*. Brochure, Market Scope, St. Louis, MO. **https://www.market-scope.com/files/products/brochures/167/2020%20Cataract%20Atlas%20Brochure%20Final.pdf**
31. Zvornicanin J, Zvornicanin E. 2018. Premium intraocular lenses: the past, present and future. *J. Curr. Ophthalmol.* 30:287–96
32. Kanclerz P, Toto F, Grzybowski A, Alio JL. 2020. Extended depth-of-field intraocular lenses: an update. *Asia Pac. J. Ophthalmol.* 9:194–202
33. Bellucci R. 2013. An introduction to intraocular lenses: material, optics, haptics, design and aberration. *Cataract* 3:38–55
34. Werner L. 2008. Biocompatibility of intraocular lens materials. *Curr. Opin. Ophthalmol.* 19:41–49
35. Harman FE, Maling S, Kampougeris G, Langan L, Khan I, et al. 2008. Comparing the 1CU accommodative, multifocal, and monofocal intraocular lenses: a randomized trial. *Ophthalmology* 115:993–1001.e2
36. Alió JL, Alió Del Barrio JL, Vega-Estrada A. 2017. Accommodative intraocular lenses: Where are we and where we are going? *Eye Vis.* 4:16

37. de la Hoz A, Germann J, Martinez-Enriquez E, Pascual D, Bekesi N, et al. 2019. Design and ex situ performance of a shape-changing accommodating intraocular lens. *Optica* 6:1050–57
38. Barbero S, Marcos S, Jimenéz-Alfaro I. 2003. Optical aberrations of intraocular lenses measured in vivo and in vitro. *J. Opt. Soc. Am. A Opt. Image Sci. Vis.* 20:1841–51
39. Artal P, Marcos S, Fonolla Navarro R, Miranda I, Ferro M. 1995. Through focus image quality of eyes implanted with monofocal and multifocal intraocular lenses. *Opt. Eng.* 34(3):772–79. **https://doi.org/10.1117/12.191818**
40. Vega F, Alba-Bueno F, Millán MS. 2011. Energy distribution between distance and near images in apodized diffractive multifocal intraocular lenses. *Investig. Ophthalmol. Vis. Sci.* 52:5695–701
41. Terwee T, Weeber H, van der Mooren M, Piers P. 2008. Visualization of the retinal image in an eye model with spherical and aspheric, diffractive, and refractive multifocal intraocular lenses. *J. Refract. Surg.* 24:223–32
42. Kim MJ, Zheleznyak L, MacRae S, Tchah H, Yoon G. 2011. Objective evaluation of through-focus optical performance of presbyopia-correcting intraocular lenses using an optical bench system. *J. Cataract Refract. Surg.* 37:1305–12
43. Gatinel D, Houbrechts Y. 2013. Comparison of bifocal and trifocal diffractive and refractive intraocular lenses using an optical bench. *J. Cataract Refract. Surg.* 39:1093–99
44. Vinas M, Benedi-Garcia C, Aissati S, Pascual D, Akondi V, et al. 2019. Visual simulators replicate vision with multifocal lenses. *Sci. Rep.* 9:1539
45. Fritz KJ, Partamian LG, Leveille AS, Kiernan JP. 1981. Intraocular lens power formulas. *Ophthalmology* 88:432–33
46. Holladay JT, Prager TC, Chandler TY, Musgrove KH, Lewis JW, Ruiz RS. 1988. A three-part system for refining intraocular lens power calculations. *J. Cataract Refract. Surg.* 14:17–24
47. Retzlaff JA, Sanders DR, Kraff MC. 1990. Development of the SRK/T intraocular lens implant power calculation formula. *J. Cataract Refract. Surg.* 16:333–40
48. Hoffer KJ. 1993. The Hoffer Q formula: a comparison of theoretic and regression formulas. *J. Cataract Refract. Surg.* 19:700–12
49. Haigis W, Lege B, Miller N, Schneider B. 2000. Comparison of immersion ultrasound biometry and partial coherence interferometry for intraocular lens calculation according to Haigis. *Graefe's Arch. Clin. Exp. Ophthalmol.* 238:765–73
50. Olsen T, Corydon L, Gimbel H. 1995. Intraocular lens power calculation with an improved anterior chamber depth prediction algorithm. *J. Cataract Refract. Surg.* 21:313–19
51. Olsen T. 2006. Prediction of the effective postoperative (intraocular lens) anterior chamber depth. *J. Cataract Refract. Surg.* 32:419–24
52. Lee AC, Qazi MA, Pepose JS. 2008. Biometry and intraocular lens power calculation. *Curr. Opin. Ophthalmol.* 19:13–17
53. Barrett GD. 1993. An improved universal theoretical formula for intraocular lens power prediction. *J. Cataract Refract. Surg.* 19:713–20
54. Aristodemou P, Knox Cartwright NE, Sparrow JM, Johnston RL. 2011. Formula choice: Hoffer Q, Holladay 1, or SRK/T and refractive outcomes in 8108 eyes after cataract surgery with biometry by partial coherence interferometry. *J. Cataract Refract. Surg.* 37:63–71
55. Aramberri J. 2003. Intraocular lens power calculation after corneal refractive surgery: double-K method. *J. Cataract Refract. Surg.* 29:2063–68
56. Waring GO IV. 2013. Diagnosis and treatment of dysfunctional lens syndrome. *Cataract Refract. Surg. Today.* **https://crstoday.com/articles/2013-mar/diagnosis-and-treatment-of-dysfunctional-lens-syndrome/**
57. Sawides L, de Gracia P, Dorronsoro C, Webster M, Marcos S. 2011. Adapting to blur produced by ocular high-order aberrations. *J. Vis.* 11(7):21. **https://doi.org/10.1167/11.7.21**
58. Marcos S, Werner JS, Burns SA, Merigan WH, Artal P, et al. 2017. Vision science and adaptive optics, the state of the field. *Vis. Res.* 132:3–33
59. Chylack LT Jr., Wolfe JK, Singer DM, Leske MC, Bullimore MA, et al. 1993. The Lens Opacities Classification System III. The Longitudinal Study of Cataract study group. *Arch. Ophthalmol.* 111:831–36

60. Santamaría J, Artal P, Bescós J. 1987. Determination of the point-spread function of human eyes using a hybrid optical-digital method. *J. Opt. Soc. Am. A Opt. Image Sci. Vis.* 4:1109–14
61. Artal P, Benito A, Pérez GM, Alcón E, De Casas A, et al. 2011. An objective scatter index based on double-pass retinal images of a point source to classify cataracts. *PLOS ONE* 6:e16823
62. Sahin O, Pennos A, Ginis H, Hervella L, Villegas EA, et al. 2016. Optical measurement of straylight in eyes with cataract. *J. Refract. Surg.* 32:846–50
63. de Castro A, Benito A, Manzanera S, Mompeán J, Cañizares B, et al. 2018. Three-dimensional cataract crystalline lens imaging with swept-source optical coherence tomography. *Investig. Ophthalmol. Vis. Sci.* 59:897–903
64. Grulkowski I, Manzanera S, Cwiklinski L, Mompeán J, de Castro A, et al. 2018. Volumetric macro- and micro-scale assessment of crystalline lens opacities in cataract patients using long-depth-range swept source optical coherence tomography. *Biomed. Opt. Express* 9:3821–33
65. Grulkowski I, Manzanera S, Cwiklinski L, Sobczuk F, Karnowski K, Artal P. 2018. Swept source optical coherence tomography and tunable lens technology for comprehensive imaging and biometry of the whole eye. *Optica* 5:52–59
66. McLeod SD, Vargas LG, Portney V, Ting A. 2007. Synchrony dual-optic accommodating intraocular lens. Part 1: optical and biomechanical principles and design considerations. *J. Cataract Refract. Surg.* 33:37–46
67. Sheppard AL, Bashir A, Wolffsohn JS, Davies LN. 2010. Accommodating intraocular lenses: a review of design concepts, usage and assessment methods. *Clin. Exp. Optom.* 93:441–52
68. Martinez-Enriquez E, Pérez-Merino P, Durán-Poveda S, Jiménez-Alfaro I, Marcos S. 2018. Estimation of intraocular lens position from full crystalline lens geometry: towards a new generation of intraocular lens power calculation formulas. *Sci. Rep.* 8:9829
69. Rosales P, Dubbelman M, Marcos S, van der Heijde R. 2006. Crystalline lens radii of curvature from Purkinje and Scheimpflug imaging. *J. Vis.* 6(10):1057–67
70. Cook CA, Koretz JF, Pfahnl A, Hyun J, Kaufman PL. 1994. Aging of the human crystalline lens and anterior segment. *Vis. Res.* 34:2945–54
71. Dubbelman M, Van der Heijde GL. 2001. The shape of the aging human lens: curvature, equivalent refractive index and the lens paradox. *Vis. Res.* 41:1867–77
72. Dubbelman M, Van der Heijde GL, Weeber HA. 2005. Change in shape of the aging human crystalline lens with accommodation. *Vis. Res.* 45:117–32
73. Rosales P, Marcos S. 2009. Pentacam Scheimpflug quantitative imaging of the crystalline lens and intraocular lens. *J. Refract. Surg.* 25:421–28
74. Kasthurirangan S, Markwell EL, Atchison DA, Pope JM. 2011. MRI study of the changes in crystalline lens shape with accommodation and aging in humans. *J. Vis.* 11(3):19. **https://doi.org/10.1167/11.3.19**
75. Sheppard AL, Evans CJ, Singh KD, Wolffsohn JS, Dunne MC, Davies LN. 2011. Three-dimensional magnetic resonance imaging of the phakic crystalline lens during accommodation. *Investig. Ophthalmol. Vis. Sci.* 52:3689–97
76. Ramasubramanian V, Glasser A. 2015. Objective measurement of accommodative biometric changes using ultrasound biomicroscopy. *J. Cataract Refract. Surg.* 41:511–26
77. Ortiz S, Siedlecki D, Grulkowski I, Remon L, Pascual D, et al. 2010. Optical distortion correction in optical coherence tomography for quantitative ocular anterior segment by three-dimensional imaging. *Opt. Express* 18:2782–96
78. Ortiz S, Pérez-Merino P, Gambra E, de Castro A, Marcos S. 2012. In vivo human crystalline lens topography. *Biomed. Opt. Express* 3:2471–88
79. Gambra E, Ortiz S, Pérez-Merino P, Gora M, Wojtkowski M, Marcos S. 2013. Static and dynamic crystalline lens accommodation evaluated using quantitative 3-D OCT. *Biomed. Opt. Express* 4:1595–609
80. Pérez-Merino P, Velasco-Ocana M, Martinez-Enriquez E, Marcos S. 2015. OCT-based crystalline lens topography in accommodating eyes. *Biomed. Opt. Express* 6:5039–54
81. Martinez-Enriquez E, Sun M, Velasco-Ocana M, Birkenfeld J, Pérez-Merino P, Marcos S. 2016. Optical coherence tomography based estimates of crystalline lens volume, equatorial diameter, and plane position. *Investig. Ophthalmol. Vis. Sci.* 57:OCT600–10

82. Sun M, Pérez-Merino P, Martinez-Enriquez E, Velasco-Ocana M, Marcos S. 2016. Full 3-D OCT-based pseudophakic custom computer eye model. *Biomed. Opt. Express* 7:1074–88
83. Martinez-Enriquez E, Pérez-Merino P, Velasco-Ocana M, Marcos S. 2017. OCT-based full crystalline lens shape change during accommodation in vivo. *Biomed. Opt. Express* 8:918–33
84. Muralidharan G, Martinez-Enriquez E, Birkenfeld J, Velasco-Ocana M, Pérez-Merino P, Marcos S. 2019. Morphological changes of human crystalline lens in myopia. *Biomed. Opt. Express* 10:6084–95
85. Martinez-Enriquez E, De Castro A, Marcos S. 2020. Eigenlenses: a new model for full crystalline lens shape representation and its applications. *Biomed. Opt. Express* 11(10):5633–49
86. Olsen T, Hoffmann P. 2014. C constant: new concept for ray tracing-assisted intraocular lens power calculation. *J. Cataract Refract. Surg.* 40:764–73
87. Olsen T. 2007. Calculation of intraocular lens power: a review. *Acta Ophthalmol. Scand.* 85:472–85
88. Shammas HJ, Shammas MC. 2015. Improving the preoperative prediction of the anterior pseudophakic distance for intraocular lens power calculation. *J. Cataract Refract. Surg.* 41:2379–86
89. Erb-Eigner K, Hirnschall N, Hackl C, Schmidt C, Asbach P, Findl O. 2015. Predicting lens diameter: ocular biometry with high-resolution MRI. *Investig. Ophthalmol. Vis. Sci.* 56:6847–54
90. Yoo YS, Whang WJ, Hwang KY, Lazo M, Hwang JH, et al. 2019. Use of the crystalline lens equatorial plane as a new parameter for predicting postoperative intraocular lens position. *Am. J. Ophthalmol.* 198:17–24
91. Melles RB, Holladay JT, Chang WJ. 2018. Accuracy of intraocular lens calculation formulas. *Ophthalmology* 125:169–78
92. Yoo YS, Whang WJ, Kim HS, Joo CK, Yoon G. 2019. Preoperative biometric measurements with anterior segment optical coherence tomography and prediction of postoperative intraocular lens position. *Medicine* 98:e18026
93. Yoo YS, Whang WJ, Kim HS, Joo CK, Yoon G. 2020. New IOL formula using anterior segment three-dimensional optical coherence tomography. *PLOS ONE* 15:e0236137
94. Tabernero J, Piers P, Benito A, Redondo M, Artal P. 2006. Predicting the optical performance of eyes implanted with IOLs to correct spherical aberration. *Investig. Ophthalmol. Vis. Sci.* 47:4651–58
95. Rosales P, Marcos S. 2007. Customized computer models of eyes with intraocular lenses. *Opt. Express* 15:2204–18
96. Pérez-Merino P, Velasco-Ocana M, Martinez-Enriquez E, Revuelta L, McFadden SA, Marcos S. 2017. Three-dimensional OCT based guinea pig eye model: relating morphology and optics. *Biomed. Opt. Express* 8:2173–84
97. Llorente L, Barbero S, Merayo J, Marcos S. 2004. Total and corneal optical aberrations induced by laser in situ keratomileusis for hyperopia. *J. Refract. Surg.* 20:203–16
98. Preussner PR, Wahl J, Weitzel D. 2005. Topography-based intraocular lens power selection. *J. Cataract Refract. Surg.* 31:525–33
99. Canovas C, Artal P. 2011. Customized eye models for determining optimized intraocular lenses power. *Biomed. Opt. Express* 2:1649–62
100. Alarcon A, Canovas C, Rosen R, Weeber H, Tsai L, et al. 2016. Preclinical metrics to predict through-focus visual acuity for pseudophakic patients. *Biomed. Opt. Express* 7:1877–88
101. Ortiz S, Siedlecki D, Pérez-Merino P, Chia N, de Castro A, et al. 2011. Corneal topography from spectral optical coherence tomography (sOCT). *Biomed. Opt. Express* 2:3232–47
102. Marcos S, Ortiz S, Pérez-Merino P, Birkenfeld J, Durán S, Jiménez-Alfaro I. 2014. Three-dimensional evaluation of accommodating intraocular lens shift and alignment in vivo. *Ophthalmology* 121:45–55
103. Ortiz S, Pérez-Merino P, Durán S, Velasco-Ocana M, Birkenfeld J, et al. 2013. Full OCT anterior segment biometry: an application in cataract surgery. *Biomed. Opt. Express* 4:387–96
104. Sun M, de Castro A, Ortiz S, Pérez-Merino P, Birkenfeld J, Marcos S. 2014. Intraocular lens alignment from an en face optical coherence tomography image Purkinje-like method. *Opt. Eng.* 53:061704
105. Marcos S, Rosales P, Llorente L, Jiménez-Alfaro I. 2007. Change in corneal aberrations after cataract surgery with 2 types of aspherical intraocular lenses. *J. Cataract Refract. Surg.* 33:217–26
106. De Castro A, Martinez-Enriquez E, Velasco-Ocana M, Duran S, Jiménez-Alfaro I, Marcos S. 2019. Intra-ocular lens power calculation using 3D OCT-based personalized computer eye models. *Investig. Ophthalmol. Vis. Sci.* 60:6463

107. Fernández EJ, Iglesias I, Artal P. 2001. Closed-loop adaptive optics in the human eye. *Opt. Lett.* 26:746–48
108. Fernández EJ, Manzanera S, Piers P, Artal P. 2002. Adaptive optics visual simulator. *J. Refract. Surg.* 18:S634–38
109. Artal P, Chen L, Fernández EJ, Singer B, Manzanera S, Williams DR. 2004. Neural compensation for the eye's optical aberrations. *J. Vis.* 4(4):281–87
110. Prieto PM, Fernández EJ, Manzanera S, Artal P. 2004. Adaptive optics with a programmable phase modulator: applications in the human eye. *Opt. Express* 12:4059–71
111. Piers PA, Manzanera S, Prieto PM, Gorceix N, Artal P. 2007. Use of adaptive optics to determine the optimal ocular spherical aberration. *J. Cataract Refract. Surg.* 33:1721–26
112. Fernández EJ, Prieto PM, Artal P. 2009. Binocular adaptive optics visual simulator. *Opt. Lett.* 34:2628–30
113. Schwarz C, Prieto PM, Fernández EJ, Artal P. 2011. Binocular adaptive optics vision analyzer with full control over the complex pupil functions. *Opt. Lett.* 36:4779–81
114. Schwarz C, Cánovas C, Manzanera S, Weeber H, Prieto PM, et al. 2014. Binocular visual acuity for the correction of spherical aberration in polychromatic and monochromatic light. *J. Vis.* 14(2):8. **https://doi.org/10.1167/14.2.8**
115. Artal P. 2014. Optics of the eye and its impact in vision: a tutorial. *Adv. Opt. Photon.* 6:340–67
116. Piers PA, Fernandez EJ, Manzanera S, Norrby S, Artal P. 2004. Adaptive optics simulation of intraocular lenses with modified spherical aberration. *Investig. Ophthalmol. Vis. Sci.* 45:4601–10
117. Leray B, Cassagne M, Soler V, Villegas EA, Triozon C, et al. 2015. Relationship between induced spherical aberration and depth of focus after hyperopic LASIK in presbyopic patients. *Ophthalmology* 122:233–43
118. Shetty N, Kochar S, Paritekar P, Artal P, Shetty R, et al. 2019. Patient-specific determination of change in ocular spherical aberration to improve near and intermediate visual acuity of presbyopic eyes. *J. Biophoton.* 12:e201800259
119. Hervella L, Villegas EA, Robles C, Artal P. 2020. Spherical aberration customization to extend the depth of focus with a clinical adaptive optics visual simulator. *J. Refract. Surg.* 36:223–29
120. Williams D, Yoon GY, Porter J, Guirao A, Hofer H, Cox I. 2000. Visual benefit of correcting higher order aberrations of the eye. *J. Refract. Surg.* 16:S554–59
121. Sawides L, Gambra E, Pascual D, Dorronsoro C, Marcos S. 2010. Visual performance with real-life tasks under adaptive-optics ocular aberration correction. *J. Vis.* 10(5):19
122. Liang J, Williams DR, Miller DT. 1997. Supernormal vision and high-resolution retinal imaging through adaptive optics. *J. Opt. Soc. Am. A Opt. Image Sci. Vis.* 14:2884–92
123. Marcos S, Sawides L, Gambra E, Dorronsoro C. 2008. Influence of adaptive-optics ocular aberration correction on visual acuity at different luminances and contrast polarities. *J. Vis.* 8(13):1
124. de Gracia P, Marcos S, Mathur A, Atchison DA. 2011. Contrast sensitivity benefit of adaptive optics correction of ocular aberrations. *J. Vis.* 11(12):5. **https://doi.org/10.1167/11.12.5**
125. Sabesan R, Zheleznyak L, Yoon G. 2012. Binocular visual performance and summation after correcting higher order aberrations. *Biomed. Opt. Express* 3:3176–89
126. Zheleznyak L, Sabesan R, Oh J-S, MacRae S, Yoon G. 2013. Modified monovision with spherical aberration to improve presbyopic through-focus visual performance. *Investig. Ophthalmol. Vis. Sci.* 54:3157–65
127. Villa C, Gutiérrez R, Jiménez JR, González-Méijome JM. 2007. Night vision disturbances after successful LASIK surgery. *Br. J. Ophthalmol.* 91:1031–37
128. Zheleznyak L, Jung H, Yoon G. 2014. Impact of pupil transmission apodization on presbyopic through-focus visual performance with spherical aberration. *Investig. Ophthalmol. Vis. Sci.* 55:70–77
129. Johannsdottir KR, Stelmach LB. 2001. Monovision: a review of the scientific literature. *Optom. Vis. Sci.* 78:646–51
130. Jiménez JR, Castro JJ, Jiménez R, Hita E. 2008. Interocular differences in higher-order aberrations on binocular visual performance. *Optom. Vis. Sci.* 85:174–79
131. Zheleznyak L, Sabesan R, Oh JS, MacRae S, Yoon G. 2013. Modified monovision with spherical aberration to improve presbyopic through-focus visual performance. *Investig. Ophthalmol. Vis. Sci.* 54:3157–65

132. Vinas M, Dorronsoro C, Cortes D, Pascual D, Marcos S. 2015. Longitudinal chromatic aberration of the human eye in the visible and near infrared from wavefront sensing, double-pass and psychophysics. *Biomed. Opt. Express* 6:948–62
133. Vinas M, Dorronsoro C, Radhakrishnan A, Benedi-Garcia C, LaVilla EA, et al. 2017. Comparison of vision through surface modulated and spatial light modulated multifocal optics. *Biomed. Opt. Express* 8:2055–68
134. Marcos S, Benedí-García C, Aissati S, Gonzalez-Ramos AM, Lago CM, et al. 2020. VioBio lab adaptive optics: technology and applications by women vision scientists. *Ophthalmic Physiol. Opt.* 40:75–87
135. Dorronsoro C, Barcala X, Gambra E, Akondi V, Sawides L, et al. 2019. Tunable lenses: dynamic characterization and fine-tuned control for high-speed applications. *Opt. Express* 27:2085–100
136. Dorronsoro C, Radhakrishnan A, Alonso-Sanz JR, Pascual D, Velasco-Ocana M, et al. 2016. Portable simultaneous vision device to simulate multifocal corrections. *Optica* 3:918–24
137. Akondi V, Dorronsoro C, Gambra E, Marcos S. 2017. Temporal multiplexing to simulate multifocal intraocular lenses: theoretical considerations. *Biomed. Opt. Express* 8:3410–25
138. de Gracia P, Dorronsoro C, Sánchez-González A, Sawides L, Marcos S. 2013. Experimental simulation of simultaneous vision. *Investig. Ophthalmol. Vis. Sci.* 54:415–22
139. Dorronsoro C, Radhakrishnan A, de Gracia P, Sawides L, Marcos S. 2016. Perceived image quality with simulated segmented bifocal corrections. *Biomed. Opt. Express* 7:4388–99
140. Radhakrishnan A, Dorronsoro C, Marcos S. 2016. Differences in visual quality with orientation of a rotationally asymmetric bifocal intraocular lens design. *J. Cataract Refract. Surg.* 42:1276–87
141. Vinas M, Aissati S, Romero M, Benedi-Garcia C, Garzon N, et al. 2019. Pre-operative simulation of post-operative multifocal vision. *Biomed. Opt. Express* 10:5801–17
142. Radhakrishnan A, Pascual D, Marcos S, Dorronsoro C. 2019. Vision with different presbyopia corrections simulated with a portable binocular visual simulator. *PLOS ONE* 14:e0221144
143. Vinas M, Aissati S, Gonzalez-Ramos AM, Romero M, Sawides L, et al. 2020. Optical and visual quality with physical and visually simulated presbyopic multifocal contact lenses. *Transl. Vis. Sci. Technol.* 9(10):20
144. Radhakrishnan A, Dorronsoro C, Sawides L, Marcos S. 2014. Short-term neural adaptation to simultaneous bifocal images. *PLOS ONE* 9:e93089
145. Sabesan R, Barbot A, Yoon G. 2017. Enhanced neural function in highly aberrated eyes following perceptual learning with adaptive optics. *Vis. Res.* 132:78–84
146. Studer HP, Riedwyl H, Amstutz CA, Hanson JV, Büchler P. 2013. Patient-specific finite-element simulation of the human cornea: a clinical validation study on cataract surgery. *J. Biomech.* 46:751–58
147. Kling S, Marcos S. 2013. Finite-element modeling of intrastromal ring segment implantation into a hyperelastic cornea. *Investig. Ophthalmol. Vis. Sci.* 54:881–89
148. Remón L, Siedlecki D, Cabeza-Gil I, Calvo B. 2018. Influence of material and haptic design on the mechanical stability of intraocular lenses by means of finite-element modeling. *J. Biomed. Opt.* 23:035003
149. Barbero S, Marcos S. 2007. Analytical tools for customized design of monofocal intraocular lenses. *Opt. Express* 15:8576–91
150. Villegas EA, Alcon E, Rubio E, Marín JM, Artal P. 2014. Refractive accuracy with light-adjustable intraocular lenses. *J. Cataract Refract. Surg.* 40:1075–84.e2
151. Debellemanière G, Flores M, Montard M, Delbosc B, Saleh M. 2016. Three-dimensional printing of optical lenses and ophthalmic surgery: challenges and perspectives. *J. Refract. Surg.* 32:201–4
152. Villegas EA, Manzanera S, Lago CM, Hervella L, Sawides L, Artal P. 2019. Effect of crystalline lens aberrations on adaptive optics simulation of intraocular lenses. *J. Refract. Surg.* 35:126–31
153. Sramka M, Slovak M, Tuckova J, Stodulka P. 2019. Improving clinical refractive results of cataract surgery by machine learning. *PeerJ* 7:e7202
154. Freeman W. 2020. *Ophthalmic surgical instruments market report: a global analysis for 2019 to 2025*. Rep., Market Scope, St. Louis, MO. **https://www.market-scope.com/pages/reports/228/2020-ophthalmic-surgical-instruments-market-report#reports**